

Lmx1b is required at multiple stages to build expansive serotonergic axon architectures

Lauren J Donovan, William C Spencer, Meagan M Kitt, Brent A Eastman, Katherine J Lobur, Kexin Jiao, Jerry Silver, Evan S Deneris*

Department of Neurosciences, School of Medicine, Case Western Reserve University, Cleveland, United States

Abstract Formation of long-range axons occurs over multiple stages of morphological maturation. However, the intrinsic transcriptional mechanisms that temporally control different stages of axon projection development are unknown. Here, we addressed this question by studying the formation of mouse serotonin (5-HT) axons, the exemplar of long-range profusely arborized axon architectures. We report that LIM homeodomain factor 1b (Lmx1b)-deficient 5-HT neurons fail to generate axonal projections to the forebrain and spinal cord. Stage-specific targeting demonstrates that Lmx1b is required at successive stages to control 5-HT axon primary outgrowth, selective routing, and terminal arborization. We show a Lmx1b→Pet1 regulatory cascade is temporally required for 5-HT arborization and upregulation of the 5-HT axon arborization gene, Protocadherin- α 2, during postnatal development of forebrain 5-HT axons. Our findings identify a temporal regulatory mechanism in which a single continuously expressed transcription factor functions at successive stages to orchestrate the progressive development of long-range axon architectures enabling expansive neuromodulation.

DOI: <https://doi.org/10.7554/eLife.48788.001>

***For correspondence:**

esd@case.edu

Competing interests: The authors declare that no competing interests exist.

Funding: See page 28

Received: 24 May 2019

Accepted: 27 July 2019

Published: 29 July 2019

Reviewing editor: Anne E West, Duke University School of Medicine, United States

© Copyright Donovan et al. This article is distributed under the terms of the [Creative Commons Attribution License](https://creativecommons.org/licenses/by/4.0/), which permits unrestricted use and redistribution provided that the original author and source are credited.

Introduction

Newly generated neurons dramatically transform their morphology to establish mature circuit connectivity. Some neurons, for example interneurons, connect to local circuits and thus need to extend their axons relatively short distances. In contrast, other neuron types, such as those giving rise to neuromodulatory systems, have the capacity to extend extremely long axons to innervate distant target fields. This is well exemplified in the case of serotonin (5-HT) synthesizing neurons. 5-HT modulates the excitability of nearly all neural circuitry in the brain and spinal cord despite being produced in a relatively small population of neurons (Azevedo et al., 2009; Baker et al., 1991; Hornung, 2003). Expansive serotonergic neuromodulation is achieved through the formation of long-range highly diffuse ascending and descending projection pathways that deliver 5-HT throughout the brain and spinal cord for synaptic or non-synaptic interactions with an array of receptors (Hannon and Hoyer, 2008; Steinbusch, 1981). Despite the decades-long knowledge of 5-HT's importance as a global neuromodulator, it is not understood how these small numbers of neurons develop, over an extended period of morphological maturation, such elaborate axonal architectures.

5-HT neurons initiate axon outgrowth concomitant with their birth and onset of 5-HT synthesis (Hawthorne et al., 2010; Lidov and Molliver, 1982). Classic neuroanatomical studies have defined three successive stages, collectively spanning several weeks, in the formation of 5-HT projection pathways: primary pathway formation during which 5-HT axon outgrowth is initiated, selective pathway routing, and finally postnatal terminal arborization (Lidov and Molliver, 1982). Following primary pathway outgrowth through the medial forebrain bundle (MFB), ascending 5-HT axons

originating in the dorsal raphe (DRN), median raphe (MRN) and B9 groups of midbrain/pons 5-HT neurons are selectively routed along pre-existing fiber tracts and reach all forebrain targets at parturition in an unarborized state (Bang et al., 2012; Lidov and Molliver, 1982; Muzerelle et al., 2016). Descending 5-HT axons, originating in the medullary serotonergic clusters, raphe pallidus (RPa), raphe obscurus (ROb), and raphe magnus (RMg), enter the spinal cord via the dorsolateral and ventral funiculi. These primary projections then route medially to invade nearly all lamina of the dorsal and ventral horns as well as the intermediate zone from cervical to sacral levels (Rajaofetra et al., 1989). After the major ascending and descending projection pathways are formed, a final, entirely postnatal, stage of 5-HT projection pathway maturation ensues during which 5-HT axons originating in different anatomically defined sub-regions flourish profuse terminal arbors in complementary and topographically organized patterns (Muzerelle et al., 2016; Ren et al., 2018). Terminal arborization develops at least through the first four postnatal weeks and leaves few, if any, regions of the brain and spinal cord devoid of serotonergic input (Gagnon and Parent, 2014; Hornung, 2003; Lidov and Molliver, 1982; Maddaloni et al., 2017; Steinbusch, 1981). What are the intrinsic mechanisms that govern successive stages in the formation of long-range profusely arborized 5-HT axon projection pathways and how are they temporally coordinated? One possibility is that each stage is governed by different intrinsic regulatory factors. Alternatively, a single continuously expressed intrinsic regulator may act at successive stages to orchestrate progressive morphological maturation of 5-HT pathways.

In contrast to the poor understanding of how 5-HT axonal pathways are formed, there is substantial knowledge of the gene regulatory networks (GRNs) that generate 5-HT neurons and control acquisition of 5-HT transmitter identity (Deneris and Gaspar, 2018). The LIM homeodomain protein, *Lmx1b*, is a crucial factor in 5-HT GRNs as 5-HT neuron selective targeting of *Lmx1b* results in the failure to induce *Tph2* expression for 5-HT synthesis and *Slc6a4* expression for 5-HT reuptake (Zhao et al., 2006). This results in extremely low levels of 5-HT in the adult brain, which is associated with high neonatal mortality and several abnormal behavioral phenotypes including hyperactivity, delayed respiratory maturation, enhanced inflammatory pain sensitivity, deficient opioid analgesia, sleep regulation, and increased contextual fear memories (Dai et al., 2008; Hodges et al., 2009; Zhang et al., 2018; Zhao et al., 2007a; Zhao et al., 2007b).

Lmx1b is a continuously expressed, terminal selector-type factor in 5-HT neurons (Hobert, 2008) raising the possibility that subsequent to its initial role in the induction of 5-HT synthesis and transport it may perform additional stage specific functions in the maturation of serotonergic connectivity. However, stage specific functions of continuously expressed terminal selectors, such as *Lmx1b*, in postmitotic neuronal morphological maturation are poorly understood (Deneris and Hobert, 2014; Hobert, 2016). Here, we report that lack of *Lmx1b* results in the failure to build long-range ascending and descending 5-HT axon projection pathways. Using temporal conditional targeting approaches we dissect distinct stage-specific functions for *Lmx1b*. Our findings show that *Lmx1b* acts at successive stages to control primary pathway growth rate, selective pathway routing and terminal arborization of 5-HT axons. We identify an ascending-specific *Lmx1b*-controlled regulatory cascade that regulates selective pathway routing and then switches to control forebrain 5-HT axon arborization through stage specific expression of genes required for arborization. This study demonstrates that a single continuously expressed transcription factor, initially required for induction of 5-HT synthesis and reuptake, subsequently acts at successive stages to build the expansive axon pathway architectures enabling CNS-wide serotonergic neuromodulation.

Results

***Lmx1b* controls formation of ascending 5-HT projection pathways**

Conditional targeting of *Lmx1b* with the *Pet1-Cre* transgene results in loss of endogenous 5-HT neuron markers, *Sert*, *Tph2*, and 5-HT at E12.5 (Zhao et al., 2006). Therefore, we generated control (*Lmx1b*^{+/+;Pet1-Cre;Ai9}) and *Lmx1b* cKO (*Lmx1b*^{fl/fl;Pet1-Cre;Ai9}) mice in which the Ai9 reporter allele was used as a surrogate marker to specifically label *Pet1*⁺ cell bodies and their axons with red fluorescent protein, TdTomato. In control adult mice, 82% of *Tph2*⁺ neurons in the DRN and MRN express TdTomato. Conversely, approximately 88% of TdTomato⁺ cells co-label with *Tph2*; the remaining

TdTomato⁺ cells likely express Tph2, but at a level insufficient for detection with standard IHC (Deneris and Gaspar, 2018; Okaty et al., 2015) (Figure 1—figure supplement 1A,B).

TdTomato⁺ cells were not found outside of the raphe nuclei (Figure 1—figure supplement 1B). TdTomato⁺ axons in control mice were widely distributed throughout the adult brain and colocalized with 5-HT (Figure 1—figure supplement 1C,D). The pattern of TdTomato⁺ axons in the control forebrain corresponded closely with the pattern of 5-HT axon distribution previously determined in the rat with an anti-5-HT antibody (Lidov and Molliver, 1982; Steinbusch, 1981). Similarly, TdTomato⁺ axon distribution in control brains was highly concordant with 5-HT axon projection patterns determined more recently using a mouse line in which GFP was knocked into the Tph2 coding region, thus validating our surrogate marking of 5-HT axons using a soluble reporter (Migliarini et al., 2013).

Abundant numbers of TdTomato⁺ cell bodies were detected in each of the raphe nuclei of *Lmx1bcKO* animals (Figure 1—figure supplement 1E). The vast majority of *Lmx1bcKO* TdTomato⁺ cells did not co-express *Lmx1b* or Tph2 (Figure 1—figure supplement 1E,F). Further, RT-qPCR analyses verified severe deficits of *Lmx1b* and *Tph2* mRNAs in flow sorted YFP-labeled Pet1⁺ neurons in *Lmx1bcKO* mice, confirming appropriate *Lmx1b* targeting (Figure 1—figure supplement 1G). Counts of TdTomato⁺ cell bodies in *Lmx1bcKO* mice indicated that equivalent numbers were present compared to controls at 3 months and that their numbers remained stable for at least 13 months (Figure 1—figure supplement 1H,I). *Lmx1bcKO* TdTomato⁺ cell bodies were located within the normal cytoarchitectural boundaries of the raphe nuclei with a mildly altered distribution and smaller size (Figure 1—figure supplement 1I,J). Together, these data indicate specific fluorescent labeling of 5-HT neurons with Ai9 and efficient *Lmx1b* knock-down in *Lmx1bcKO* animals.

Analysis of TdTomato⁺ axons in adult *Lmx1bcKO* mice revealed a dramatically different pattern compared to that in control mice (Figure 1A,B). Although TdTomato⁺ axons were present in normal density and with proper ascending trajectory within the MFB of *Lmx1bcKO* mice, TdTomato⁺ axons were nearly completely missing throughout the forebrain of *Lmx1bcKO* animals distal to the thalamus (Figure 1B). Indeed, the vast majority of TdTomato⁺ axons failed to reach various distal fiber tracts including the fimbria-fornix, supracallosal stria, cingulum bundle, and olfactory tract (Figure 1B). Consequently, few if any TdTomato⁺ axons were present in the olfactory bulb, cortex, amygdala, hippocampus, striatum or many regions of the hypothalamus (Figure 1B–D; Figure 1—figure supplement 2A,B). It is likely that the few TdTomato⁺ 5-HT axons that did reach the distal forebrain were the result of a small number of 5-HT neurons in which Ai9 expression was activated, but *Lmx1b* targeting failed (Figure 1—figure supplement 1F).

Although *Lmx1bcKO* TdTomato⁺ axons were present in the thalamus, the distribution of their terminal arbors was quite different from that in controls (Figure 1B,E). We found aberrant clumping of mutant TdTomato⁺ terminal arbors in several intralaminar thalamic nuclei (Figure 1E; Figure 1—figure supplement 2C). Many regions were completely devoid of arbors unlike the relatively homogeneously tiled distribution in the control thalamus (Figure 1E, arrowheads). In addition, the conspicuously dense 5-HT arborization that demarcates the paraventricular nucleus of the thalamus (PVT) was completely absent in *Lmx1bcKO* mice (Figure 1E; Figure 1—figure supplement 2D).

To verify the deficit of TdTomato⁺ axons in the forebrain of *Lmx1bcKO* mice, we performed a second method of axon labeling by stereotaxic injection of an AAV2 virus expressing a Cre-dependent membrane bound channelrhodopsin with a YFP tag (rAAV2/Ef1a-DIO-hChR2-EYFP) into the midbrain of adult control and *Lmx1bcKO* mice. In *Lmx1bcKO* mice, we found an absence of YFP⁺ axons in all of the distal areas in which TdTomato⁺ axons were absent. Moreover, YFP⁺ axons were colocalized in all forebrain areas with TdTomato⁺ axons (Figure 1—figure supplement 1K,L).

Lmx1b controls formation of descending 5-HT projection pathways

As *Lmx1b* is strongly expressed in all medullary raphe 5-HT neurons, we next investigated descending 5-HT axon development. In control animals, 80% of Tph2⁺ medullary cell bodies expressed TdTomato and 92% of TdTomato⁺ cell bodies were co-labeled with Tph2 (Figure 2—figure supplement 1A). TdTomato⁺ axon patterns in control E15.5 embryos corresponded closely with the pattern of developing 5-HT-labeled axons in the ventral and lateral funiculi of the spinal cord, thus indicating specific labeling of descending 5-HT axons with TdTomato (Figure 2—figure supplement 1B). In addition, the pattern of control TdTomato⁺ axon distribution throughout the embryonic and adult spinal cord corresponded to descending 5-HT axons patterns in gray and white matter

Figure 1 continued

corpus callosum; hipp, hippocampus; spt, septum; hyp, hypothalamus; thal, thalamus; sc, superior colliculus; MFB, medial forebrain bundle; DRN, dorsal raphe nucleus. Schematic (right): ot, olfactory tract; cg/SCS, cingulum/supracallosal stria; fx, fornix; sm, stria medularis; fr, fasciculus retroflexus. (C) Confocal images of TdTomato⁺ axons in sagittal sections. *Lmx1bcKO* axons failed to fill cingulum bundles or innervate the hippocampus. Scale bars, 200 μ m. cg, cingulum; cc, corpus callosum; LSM, lacunosum moleculare; DG, dentate gyrus; CA1 of hippocampus. (D) Coronal sections of cortex show near complete lack of *Lmx1bcKO* TdTomato⁺ axons. Scale bars, 50 μ m. (E) Coronal view of altered patterns of TdTomato⁺ axons in *Lmx1bcKO* thalamus. Arrowheads indicate areas devoid of axons in *Lmx1bcKO* thalamus. Numbers correspond to areas of axon clumping in *Lmx1bcKO* thalamus. See **Figure 1—figure supplement 2** for high magnification images. Scale bars, 100 μ m. PVT, paraventricular nucleus of the thalamus; 3V, third ventricle.

DOI: <https://doi.org/10.7554/eLife.48788.002>

The following figure supplements are available for figure 1:

Figure supplement 1. Surrogate marking of 5-HT cell bodies and axons and *Lmx1b* conditional targeting.

DOI: <https://doi.org/10.7554/eLife.48788.003>

Figure supplement 2. *Lmx1b* deficiency disrupts 5-HT axon patterns in the forebrain.

DOI: <https://doi.org/10.7554/eLife.48788.004>

described in the rat and mouse with an anti-5-HT antibody (Ballion et al., 2002; Rajaofetra et al., 1989). We confirmed that the number of TdTomato-labeled Pet1⁺ neurons in the medullary raphe nuclei did not differ between *Lmx1bcKO* and control mice at 3 months of age (Figure 2—figure supplement 1C). Further, *Lmx1bcKO* TdTomato⁺ cells did not express Tph2, confirming targeting of *Lmx1b* (Figure 2—figure supplement 1D).

We found a severe lack of TdTomato⁺ axons in the white matter funiculi, through which 5-HT axon projections normally extend caudally through the spinal cord (Figure 2A; Figure 2—figure supplement 2A). In addition, a severe reduction of *Lmx1bcKO* TdTomato⁺ axons was found in gray matter at all levels of the spinal cord (Figure 2A). The normally dense innervation to the dorsal and ventral horns of control spinal cords was dramatically decreased in cervical, thoracic and lumbar levels in *Lmx1bcKO* mice (Figure 2A; Figure 2—figure supplement 2B,C). At cervical levels there was a 67% deficit of TdTomato⁺ axons in white matter while at lumbar levels there was a 92% deficit (Figure 2B). Quantitation of TdTomato⁺ axons in gray matter revealed a progressive cervical to lumbar deficit, 73% and 94%, respectively in *Lmx1bcKO* cords compared to control cords (Figure 2C). Collectively, our results indicate that *Lmx1b* deficiency severely disrupts long-range 5-HT axon architecture in the forebrain and spinal cord and that the deficit becomes increasingly profound with increasing distance from 5-HT cell bodies.

Delayed primary pathway formation and aborted selective pathway routing in *Lmx1bcKO* mice

We next followed the development of *Lmx1bcKO* TdTomato⁺ axons to distinguish among several possible explanations for the dramatic defects in ascending and descending 5-HT axon pathways: i, disrupted primary pathway formation; ii, failure to selectively route axons through pre-existing tracts; iii, abnormal axon trajectories with subsequent failure to extend, iv, normal pathway development followed by dieback. We first investigated TdTomato⁺ axons at E13.5 when primary pathway formation is underway and *Lmx1b* conditional targeting has occurred. At this stage, TdTomato⁺ axon outgrowth and trajectory in *Lmx1bcKO* mice were normal as they coursed through the MFB over the mesencephalic flexure (Figure 3A). At E16.5, however, *Lmx1bcKO* TdTomato⁺ axons exhibited a clear failure to extend as far rostrally as control axons, suggesting either aborted or delayed axon outgrowth along the more rostral portions of the MFB during late stage primary pathway formation (Figure 3B). At E18.5, the density of control TdTomato⁺ axons was maximal throughout the MFB and TdTomato⁺ axons were present as far rostral as the septum and diagonal band, where 5-HT axons turn dorsally to navigate through the cingulum, supracallosal stria, and fimbria-fornix (Figure 3C). *Lmx1bcKO* TdTomato⁺ axons now appeared at normal density throughout the MFB, thus supporting delayed axon outgrowth at E16.5 (data not shown). However, at this stage, most *Lmx1bcKO* TdTomato⁺ axons failed to turn dorsally and remained stalled within the MFB. A smaller number of *Lmx1bcKO* TdTomato⁺ axons did turn dorsally away from the MFB to pass through the septum and diagonal band (Figure 3C). Virtually all *Lmx1bcKO* axons failed to extend and selectively route into the cingulum and fimbria-fornix, thus failing to reach the cortex and hippocampus.

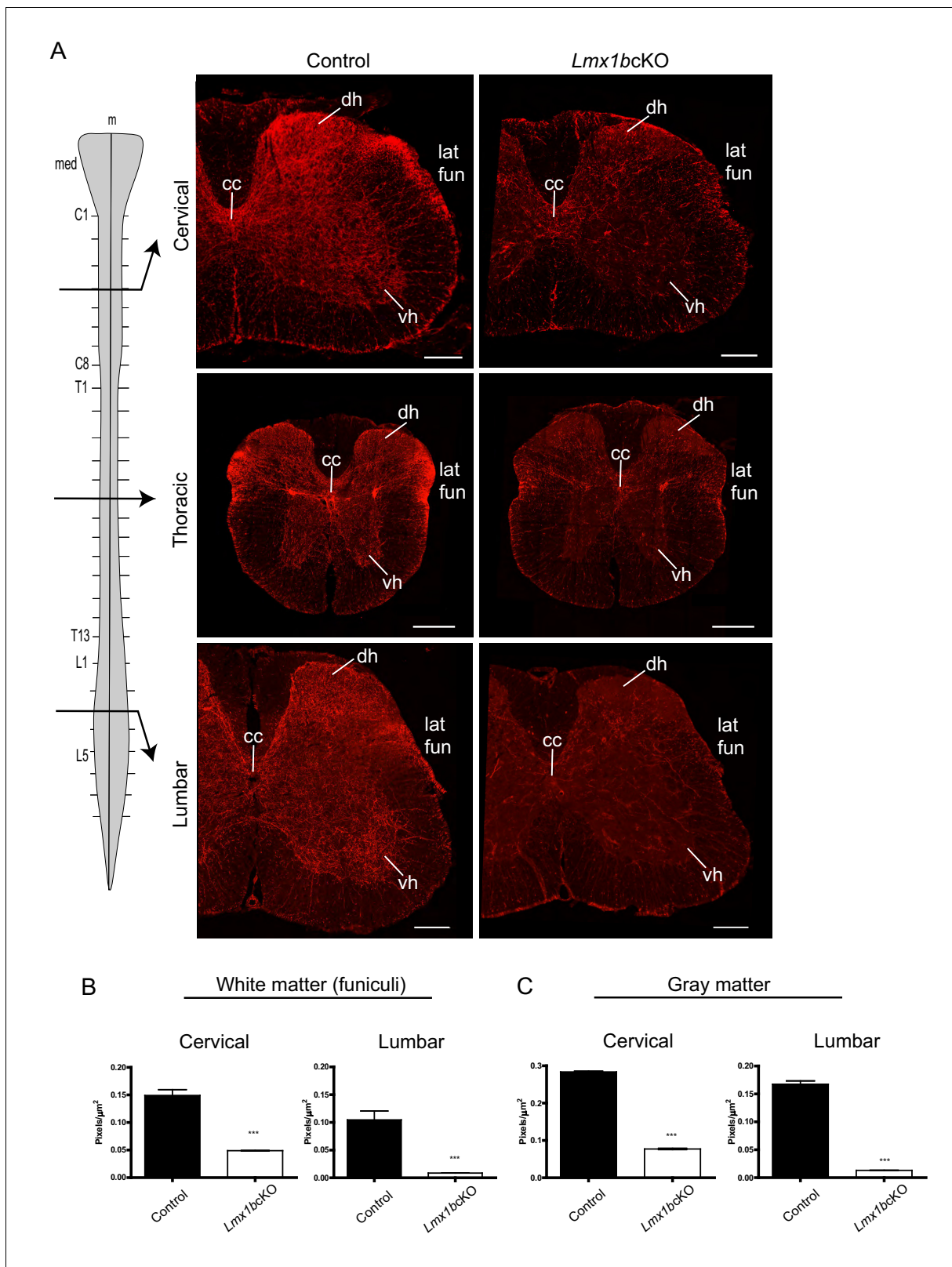


Figure 2. *Lmx1b* is required for the formation of descending 5-HT axon projection pathways. (A) Coronal sections taken at cervical (C4), thoracic (T6), and lumbar (L3) levels of the spinal cord (diagram, left). Immunolabeling for TdTomato shows *Lmx1bcKO* axons were severely reduced at every level of the cord in both gray and white matter compared to controls. Scale bars, 200 μm. m, midline; med, medulla; cc, central canal; dh, dorsal horn; vh, ventral horn; lat fun, lateral funiculi. (B, C) Quantification of total TdTomato⁺ axons (pixels/μm²) in white (B) and gray (C) matter at cervical and lumbar levels. Figure 2 continued on next page

Figure 2 continued

levels (n = 3, control; n = 3 *Lmx1bcKO* mice). Two-way ANOVA with Welch's correction, *p<0.05, **p<0.001, and ***p<0.0001. Data are represented as mean ± SEM.

DOI: <https://doi.org/10.7554/eLife.48788.005>

The following figure supplements are available for figure 2:

Figure supplement 1. Conditional targeting of *Lmx1b* in the descending 5-HT projection pathway.

DOI: <https://doi.org/10.7554/eLife.48788.006>

Figure supplement 2. Progressive deficits of 5-HT axon fibers in *Lmx1b* deficient spinal cord white and gray matter.

DOI: <https://doi.org/10.7554/eLife.48788.007>

Lmx1bcKO TdTomato⁺ axons still did not exhibit ectopic trajectories. Further examination in one-month old *Lmx1bcKO* animals revealed a similar deficit of TdTomato⁺ axons in distal forebrain tracts (data not shown). These findings suggest that conditional targeting of *Lmx1b* at E12.5 results in delayed primary pathway formation followed by a profound failure of ascending axons to selectively route into pre-existing fiber tracts.

Analysis of descending TdTomato⁺ fibers at E15.5 revealed similar initial axon outgrowth through the caudal medulla to the upper cervical spinal cord from *Lmx1bcKO* and control medullary 5-HT cell bodies (**Figure 3D**). Although *Lmx1bcKO* TdTomato⁺ axons appropriately entered the lateral and ventral funiculi of the cervical spinal cord, greatly reduced densities were evident beginning at mid-cervical levels (**Figure 3D**). At lumbar levels, *Lmx1bcKO* TdTomato⁺ axons were nearly undetectable in the lateral and ventral funiculi (**Figure 3D**). These results indicate that TdTomato⁺ axons were not able to extend into the funiculi, which caused a severe and progressive cervical to lumbar deficit of 5-HT innervation in the adult *Lmx1bcKO* spinal cord (**Figures 2 and 3D**).

Lmx1b acts temporally to control 5-HT axon selective pathways

As formation of 5-HT axon projection pathways occurs over several weeks of embryonic to early postnatal neural maturation we next sought to determine whether *Lmx1b* is temporally required for 5-HT axon pathway formation. To address this question, we developed a tamoxifen inducible targeting strategy (**Figure 4A**) to knock-down *Lmx1b* at different early postnatal timepoints. Thus, we generated *Lmx1bicKO* (*Lmx1b^{fl/fl}; Tph2-CreER; Ai9*) and iControl (*Lmx1b^{+/+}; Tph2-CreER; Ai9*) mice. Subcutaneous delivery of tamoxifen into iControl pups resulted in approximately 94% of Tph2⁺ neurons co-labeled with TdTomato in the DRN/MRN/B9 (**Figure 4—figure supplement 1A,B**). Conversely, 94% of TdTomato⁺ cells were co-labeled with Tph2 (**Figure 4—figure supplement 1B**). As with the *Pet1-Cre* driver, the *Tph2-CreER* activated TdTomato⁺ cells that are Tph2⁺ evidently express Tph2 at a low level (**Deneris and Gaspar, 2018; Okaty et al., 2015**). RT-qPCR analysis of flow sorted TdTomato⁺ cells verified that *Lmx1b* mRNA was significantly reduced in *Lmx1bicKO* mice (**Figure 4B**). Equivalent numbers of TdTomato-labeled cell bodies were generated in *Lmx1bicKO* versus iControl mice after injection of tamoxifen (**Figure 4—figure supplement 1C,D**). In contrast to *Lmx1bcKO* TdTomato⁺ cells, cell body size and distribution of tamoxifen treated *Lmx1bicKO* TdTomato⁺ cells were not different from that of iControl TdTomato⁺ cells (**Figure 4—figure supplement 1C,E**).

We analyzed TdTomato⁺ axons in P1 targeted *Lmx1bicKO* mice four weeks after tamoxifen delivery, when 5-HT axon pathways have fully matured (**Lidov and Molliver, 1982; Maddaloni et al., 2017**). We found a dramatic deficit in TdTomato⁺ arbors throughout the hippocampus in *Lmx1bicKO* mice compared to controls (**Figure 4C**). In addition, TdTomato⁺ arbors were severely reduced in all layers of the cortex with the most medial layers almost completely devoid of arbors in *Lmx1bicKO* mice (**Figure 4D**). These results clearly demonstrate that *Lmx1b* is temporally required for postnatal development of 5-HT terminal axons. However, we noticed that in addition to reduced 5-HT arbors in the hippocampus and cortex, TdTomato labeling within the supracallosal stria and cingulum, major routes to the hippocampus and cortex, were consistently less intense in P1 targeted *Lmx1bicKO* mice compared to controls (**Figure 4C, asterisk**). Indeed, further detailed examination revealed that these major 5-HT routes had not yet fully formed (**Figure 4E**). Quantification of TdTomato⁺ axons within the cingulum and supracallosal stria tracts confirmed a significant decrease in P1 targeted *Lmx1bicKO* mice compared to controls (**Figure 4F**). These results indicate that i,

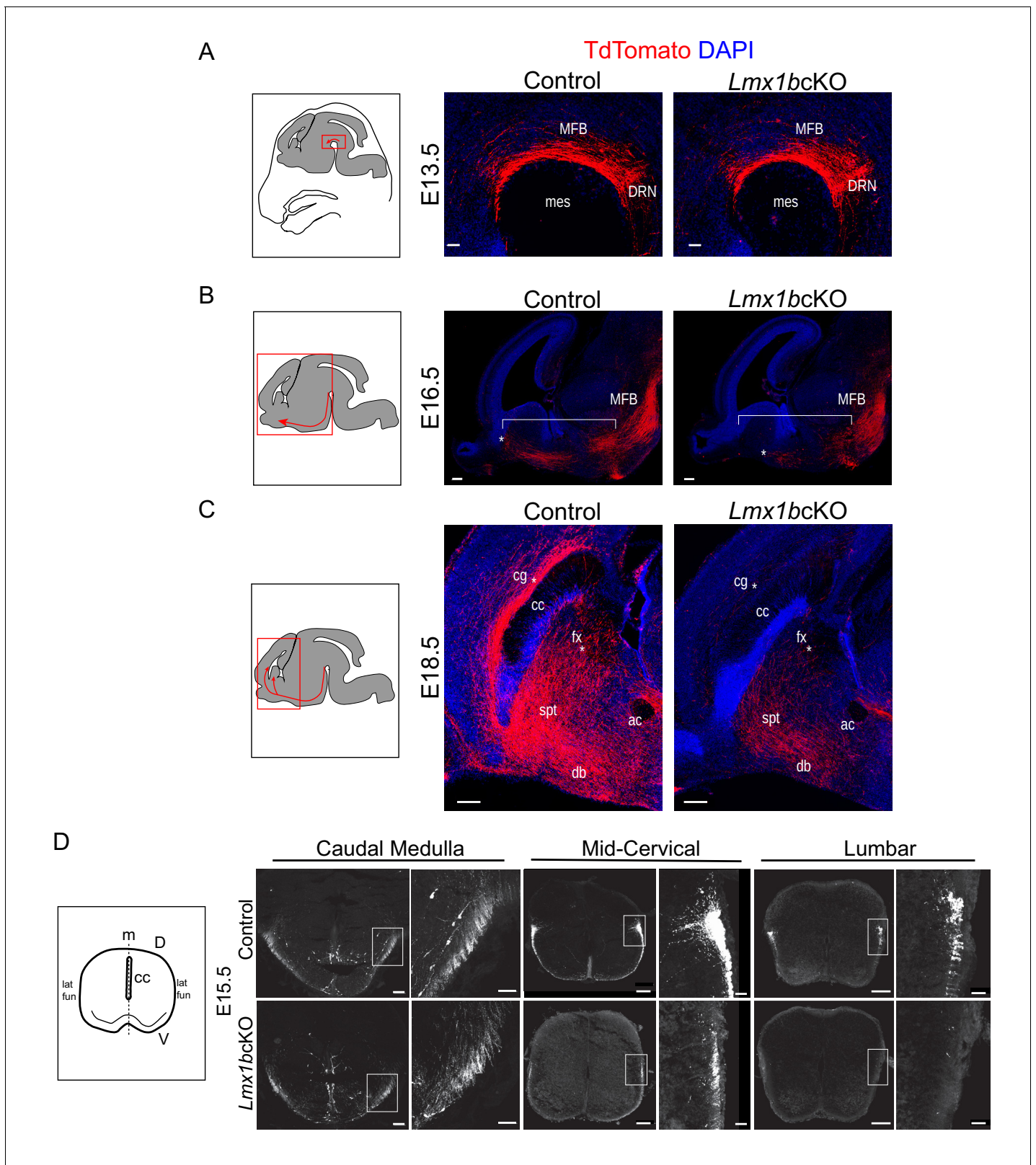


Figure 3. Initial axon outgrowth is delayed and selective pathway routing fails in *Lmx1b* deficient 5-HT neurons. (A–C) Immunolabeled TdTomato⁺ ascending axons in sagittal slices at different embryonic stages. Diagrams (left) show area of image (red box) presented for each time point. Arrows indicate direction of growing axons. E13.5 *Lmx1bcKO* axons exhibited similar ascending trajectories and densities as controls (A). E16.5 *Lmx1bcKO* axons did not extend as far (asterisk) and were less abundant (under bracket) compared to control axons (B). E18.5 *Lmx1bcKO* axons failed to fill

Figure 3 continued on next page

Figure 3 continued

multiple axon tracts (cg, fx; asterisks) compared to controls (C). Scale bars, 50 μm (A), 200 μm (B,C). DRN, dorsal raphe nucleus; MFB, medial forebrain bundle; mes, mesencephalic flexure; cg, cingulum bundle; fx, fornix; ac, anterior commissure; spt, septum; db, diagonal band; cc, corpus callosum. (D) Diagram (left) depicting coronal section of an embryonic spinal cord. TdTomato⁺ descending axons at E15.5 in control vs *Lmx1bcKO* embryos. *Lmx1bcKO* axons exit caudal medulla similar to controls but were severely reduced in funiculi at lower levels of the cord (mid-cervical and lumbar). Boxed region of lateral funiculi enlarged to the right of each image. Scale bars, 100 μm (low magnification), 50 μm (high magnification-medulla), 20 μm (high magnification- cervical/lumbar insets). Lat fun, lateral funiculi; cc, central canal; m, midline; D, dorsal; V, ventral.

DOI: <https://doi.org/10.7554/eLife.48788.008>

long-range 5-HT axon routing is continuing to develop in the early neonatal period and ii, *Lmx1b* is required at this stage for completion of 5-HT axon selective routing.

***Lmx1b* switches function to control terminal arborization**

We next targeted *Lmx1bcKO* mice at P3 to further investigate temporal requirements for *Lmx1b* (Figure 5A). Importantly, in contrast to findings obtained in P1 targeted mice, we found that the density of TdTomato-labeled fibers in the supracallosal stria was now similar in P3 targeted *Lmx1bcKO* and iControl mice (Figure 5—figure supplement 1A). Furthermore, TdTomato-labeled fibers in the cingulum, one of the longest of 5-HT forebrain tracts, was now comparable in P3 targeted *Lmx1bcKO* and iControl mice (Figure 5B). Quantification of the cingulum and supracallosal stria confirmed no significant difference between P3 targeted *Lmx1bcKO* and iControl mice (Figure 5—figure supplement 1B). These findings indicate that 5-HT axon routing was complete in P3 targeted *Lmx1bcKO* mice.

Despite fully developed 5-HT selective pathway routes in the forebrain, TdTomato⁺ arbors were significantly decreased throughout the hippocampus (Figure 5C; Figure 5—figure supplement 1B). A majority of remaining arbors detected within the hippocampus of P3 targeted *Lmx1bcKO* mice were found in the molecular layer (SLM), which are the first 5-HT arbors to appear in the hippocampus during rat development (Lidov and Molliver, 1982). TdTomato⁺ arbors were also severely decreased in all cortical layers of the P3 targeted *Lmx1bcKO* brain including in layer I and VI where axons of passage also exist (Figure 5D) (Lidov and Molliver, 1982). Quantification of the cortex confirmed a significant decrease of TdTomato⁺ axon arbors in P3 targeted *Lmx1bcKO* compared to iControls (Figure 5—figure supplement 1B). It is important to note that many 5-HT terminal arbors have already been generated in the forebrain at P3 (Lidov and Molliver, 1982; Maddaloni et al., 2017). Thus, *Lmx1b* targeting at P3 results in the failure of new arbors to form while leaving previously generated arbors intact.

Interestingly, arborization deficits were also found within the thalamus of P3 targeted *Lmx1bcKO* mice. Similar to what we observed in *Lmx1bcKO* mice, the normally dense arborization within the PVT was absent in P3 targeted *Lmx1bcKO* mice, rendering the PVT indiscernible (Figure 5E). Together, these results reveal a successive stage of continuous *Lmx1b* function during which it switches to control terminal arborization of forebrain 5-HT axons.

Targeting of 5-HT synthesis does not impair formation of forebrain and spinal cord 5-HT arbors

Lack of 5-HT itself has been reported to affect development of forebrain 5-HT terminal arbor patterns (Migliarini et al., 2013). Therefore, we next investigated whether the arborization defects present in *Lmx1b* deficient mice resulted from reduced *Tph2* expression and consequently reduced 5-HT levels. To specifically knock down *Tph2* to a level comparable to that in *Lmx1bcKO* mice, we generated *Tph2cKO* (*Tph2^{fl/fl};Pet1-Cre;Ai9*) and control (*Tph2^{+/+};Pet1-Cre;Ai9*) mice. The numbers of TdTomato⁺ cells in each raphe nuclei did not differ in *Tph2cKO* and control mice (Figure 6A). In the DRN/MRN/B9 nuclei, we found a 74% reduction of *Tph2*⁺ neurons in *Tph2cKO* compared to the 79% reduction of *Tph2*⁺ neurons in *Lmx1bcKO* mice (Figure 6B,C). Additionally, we confirmed loss of 5-HT itself in *Tph2cKO* mice (Figure 6D).

We analyzed TdTomato⁺ terminal arbors throughout the forebrain in adult *Tph2cKO* mice. We did not find differences in *Tph2cKO* versus control TdTomato-labeled arbor patterns anywhere in the forebrain including the hippocampus, cortex, and the PVT (Figure 6E). Further, despite loss of *Tph2* in medullary neurons of *Tph2cKO* mice (Figure 6F), analysis of the spinal cord from cervical to

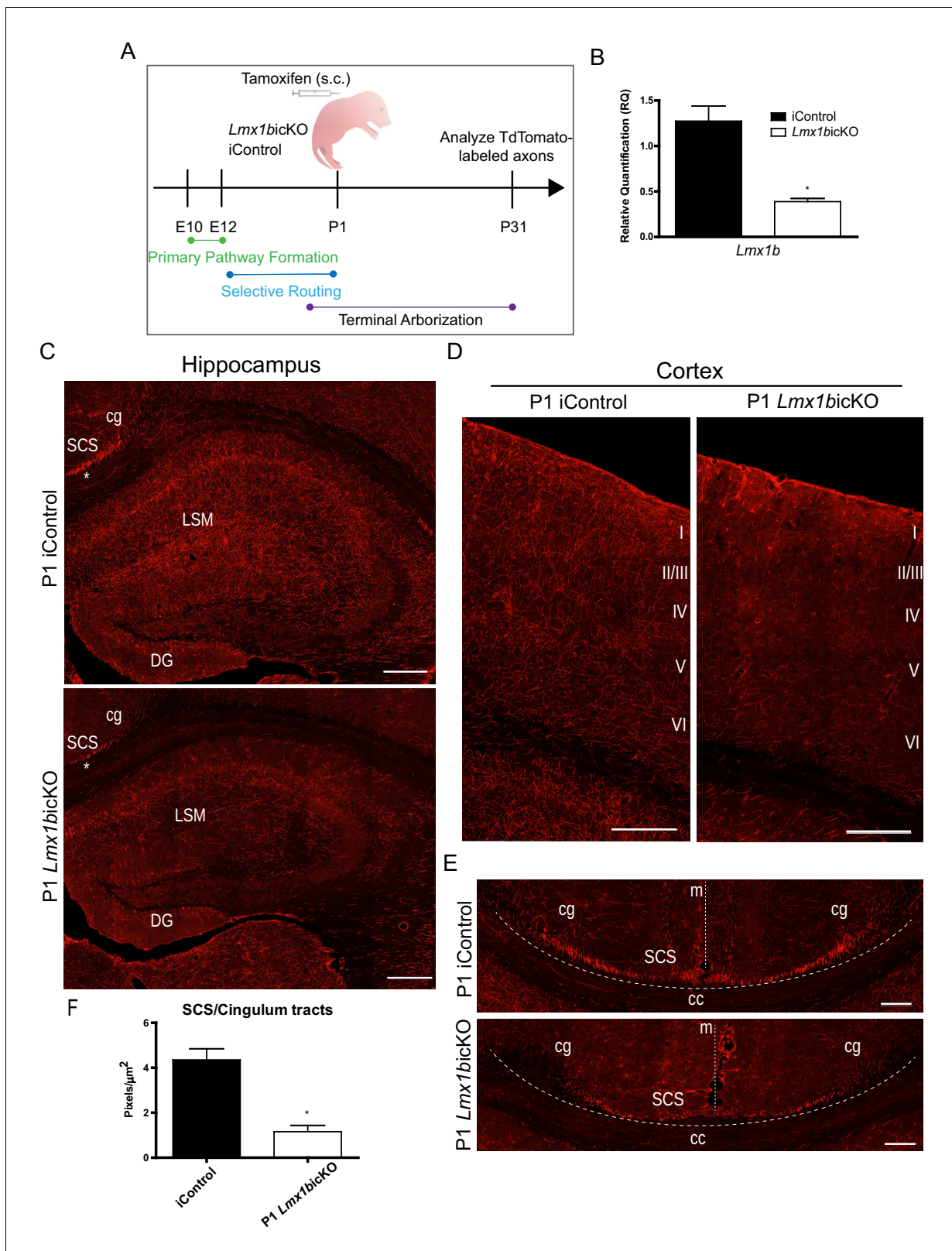


Figure 4. *Lmx1b* is temporally required for 5-HT projection pathway formation. (A) Schematic of tamoxifen-inducible approach to target *Lmx1b* at postnatal day (P)1. (B) RT-qPCR of flow sorted TdTomato⁺ neurons from postnatal targeted mice (n = 3, iControl; n = 4, *Lmx1bicKO* mice). Unpaired t-test with Welch's correction, *p<0.05. Data are represented as mean ± SEM. (C) Coronal sections of P1 targeted *Lmx1bicKO* hippocampus compared to iControls analyzed at P31. *, incomplete formation of SCS and cingulum in P1 targeted *Lmx1bicKO* brain. Scale bars, 200 μm . (D) Coronal sections of

Figure 4 continued on next page

Figure 4 continued

P1 targeted *Lmx1b*KO cortex compared to iControls analyzed at P31. Scale bars, 200 μm . (E) Coronal sections at level of corpus callosum showing incomplete formation of major 5-HT axon routes, SCS and cingulum, in P1 targeted *Lmx1b*KO forebrain compared to iControls (above dotted line). Scale bars, 100 μm . cg, cingulum; SCS, supracallosal stria; cc, corpus callosum; m, midline. (F) Quantification of axons within SCS and cingulum tracts (n = 3, iControl; n = 3, *Lmx1b*KO mice). Unpaired t-test with Welch's correction, p=0.0112. Data are represented as mean \pm SEM.

DOI: <https://doi.org/10.7554/eLife.48788.009>

The following figure supplement is available for figure 4:

Figure supplement 1. Efficiency of postnatal tamoxifen inducible targeting of *Lmx1b*.

DOI: <https://doi.org/10.7554/eLife.48788.010>

lumbar levels revealed no differences in axon densities compared to control mice (**Figure 6G**). Collectively, these results indicate that the loss of *Tph2* and thus reduced levels of 5-HT in *Lmx1b*KO or *Lmx1b*KO mice did not contribute to either the routing or arborization defects. Evidently, *Tph2* and 5-HT levels need to be reduced to a greater extent than we achieved in either our *Lmx1b*KO or our *Tph2*KO mice to generate the 5-HT arborization defects observed in mice engineered to completely eliminate *Tph2* function and brain 5-HT (**Migliarini et al., 2013**).

Lmx1b controlled axon-related transcriptomes

Genome-wide analysis of *Lmx1b* controlled serotonergic transcriptomes has not been performed and consequently only a few serotonergic genes are known *Lmx1b* targets (**Zhao et al., 2006**). We performed RNA-sequencing (RNA-seq) on flow sorted rostral hindbrain 5-HT neurons, which give rise to the ascending system, and caudal hindbrain 5-HT neurons, which give rise to the descending system, obtained from *Lmx1b*KO and control E17.5 embryos (**Figure 7A**). Differential expression analysis revealed that the known *Lmx1b* target genes, *Tph2*, *Slc18a2*, *Slc6a4*, *SCG II*, *Ctr*, were significantly decreased in our E17.5 rostral and caudal *Lmx1b*KO datasets. Moreover, we found significantly decreased expression of other 5-HT pathway genes, *Ddc*, *Slc22a3*, *Htr1a*, *Gch1*, *Gchfr*, in both rostral and caudal *Lmx1b*KO sorted 5-HT neurons that were previously unknown *Lmx1b* targets (**Figure 7B,C**).

In addition to these changes, expression of many other genes was altered in the rostral and caudal sorted neurons (**Figure 7D,E**). In rostral *Lmx1b*KO neurons, expression of 784 genes were significantly decreased, while 118 genes showed significantly increased expression (**Figure 7F,G**). In caudal *Lmx1b*KO neurons, expression of 1529 genes were significantly decreased and 772 were significantly increased (**Figure 7F,G**). Although there were many genes commonly regulated by *Lmx1b*, many more were uniquely regulated by *Lmx1b* in rostral versus caudal 5-HT neurons (**Figure 7F-H**).

Over-representation analysis of Gene Ontology (GO) terms from rostral and caudal *Lmx1b*-regulated 5-HT neuron genes revealed a pattern of strong enrichment for genes involved in axon development and morphogenesis (**Figure 7I**). In fact, the top enriched GO term, axon development, represents over 150 genes with a Benjamini-Hochberg (BH) adjusted p-value of 0. Many other axon-related terms included axon part, cell leading edge, regulation of supramolecular fiber organization, neuron projection fasciculation, tissue migration, cell-substrate adhesion, negative chemotaxis, morphogenesis of a branching structure, cell leading edge, extracellular matrix binding, and semaphorin receptor binding were enriched at $\text{FDR} \leq 0.05$. Grouping the genes from all of these axon-related categories together produced a dataset of 422 genes regulated by *Lmx1b* in rostral and/or caudal 5-HT neurons that have known roles in axon development or function (**Supplementary file 1**). Sixty-six of these downstream genes were significantly altered in both the ascending and descending 5-HT subsystems; 71 genes were uniquely altered in the ascending subsystem while 285 were uniquely altered in the descending subsystem. This analysis suggests that *Lmx1b* coordinates distinct axonal regulatory programs and transcriptomes to build the two divergent axonal subsystems.

Previous studies have implicated several effector genes in the growth and patterning of 5-HT axons (**Chen et al., 2017**; **Donovan et al., 2002**; **Fournet et al., 2010**; **Katori et al., 2017**; **Lee et al., 2005**). In most cases, however, is it not known whether these genes perform cell intrinsic functions in 5-HT neurons. Examination of our rostral and caudal RNA-seq datasets revealed significantly decreased expression of most but not all of these genes (**Figure 7J,K**). We validated the expression changes of these genes with RT-qPCR from flow-sorted E17.5 rostral 5-HT neurons (**Figure 7O**). Together, these expression studies suggest *Lmx1b* controls ascending and descending

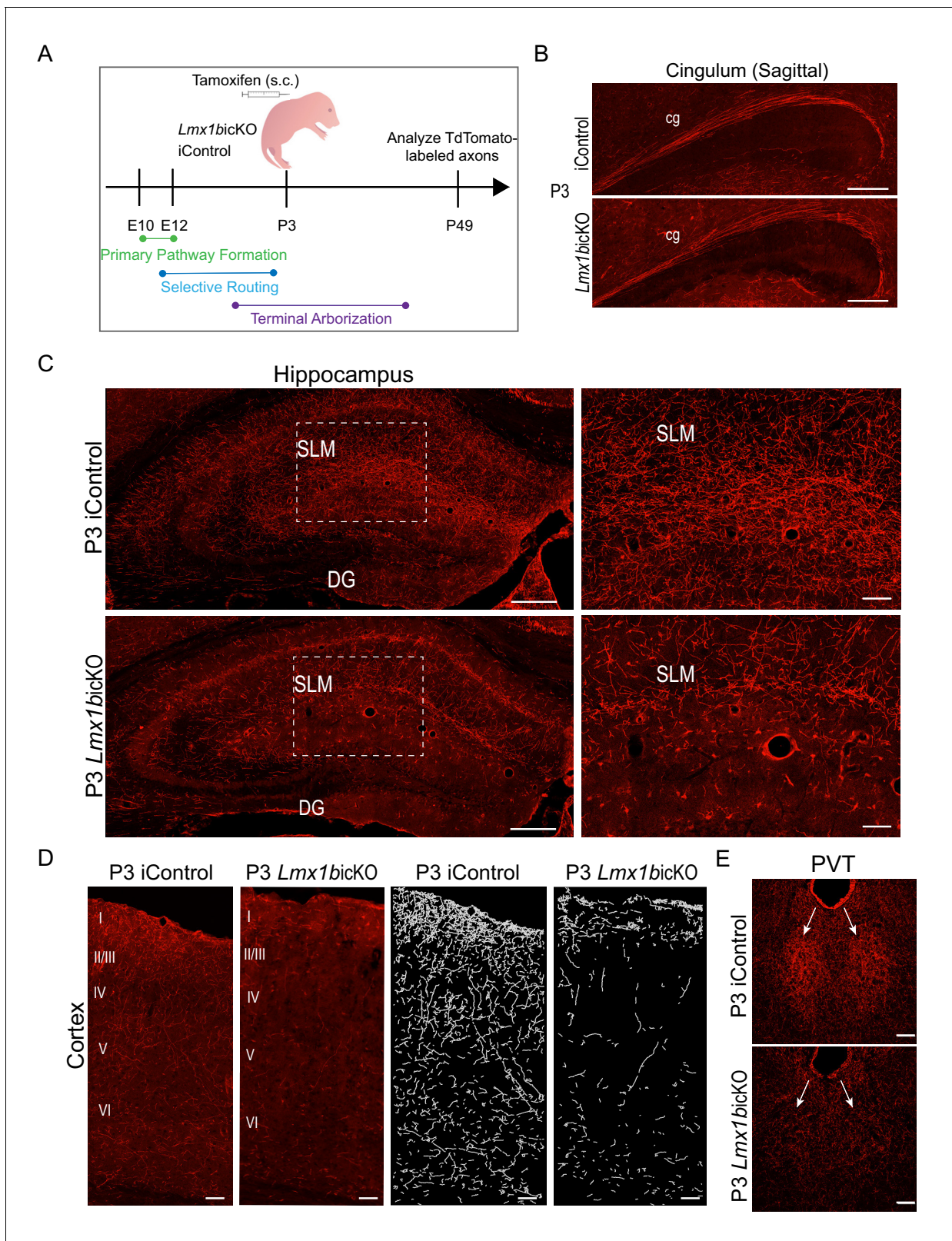


Figure 5. *Lmx1b* temporally controls postnatal 5-HT terminal arborization. (A) Schematic of tamoxifen inducible targeting of *Lmx1b* at postnatal day (P) 3. (B) Sagittal view of cingulum shows fully formed long-range axon routes in P3 targeted *Lmx1bicKO* mice compared to iControls. Scale bars, 200 μ m. (C) Coronal sections of hippocampus in P3 targeted *Lmx1bicKO* mice compared to iControls. Dashed boxed region: higher magnification image at right highlighting reduced TdTomato⁺ axons in *Lmx1bicKO* SLM. Scale bars, 200 μ m (low magnification), 50 μ m (high magnification). SLM, stratum

Figure 5 continued on next page

Figure 5 continued

lacunosum moleculare; DG, dentate gyrus. (D) Coronal sections of cortex of P3 targeted *Lmx1b*cKO mice compared to iControls. Imaris tracing; right panels. Scale bars, 100 μm . (E) Decreased TdTomato⁺ arbors detected in P3 targeted *Lmx1b*cKO PVT compared to iControls (arrows). Scale bars, 50 μm .

DOI: <https://doi.org/10.7554/eLife.48788.011>

The following figure supplement is available for figure 5:

Figure supplement 1. P3 targeted *Lmx1b*cKO mice display normal 5-HT axon routing but decreased 5-HT terminal arbors.

DOI: <https://doi.org/10.7554/eLife.48788.012>

5-HT projection pathways in part through *Gap43*, *Pcdhac2*, *Ndn*, *Ret*, *Ntrk2*, *Map6* (*STOP*), and *Celsr3* but that potentially hundreds of other functionally diverse *Lmx1b*-controlled genes are likely involved in the formation of 5-HT projection pathways (**Figure 7J,K,O**; **Supplementary file 1**).

An ascending-specific axonal *Lmx1b*→*Pet1* regulatory cascade

The regulatory interactions among transcription factors in the 5-HT GRN are poorly understood but are likely to be important for the development of 5-HT neurons. We reasoned that further study of these interactions might illuminate the regulatory mechanisms through which *Lmx1b* temporally controls formation of ascending and descending 5-HT axon pathways. Our whole genome expression analyses revealed complex effects of *Lmx1b* deficiency on the expression of other regulatory factors in the 5-HT GRN (**Figure 7L–O**). Decreased *Pet1* expression was the most consistent and persistent change among the regulatory factors in the rostral and caudal 5-HT GRNs after conditional targeting of *Lmx1b*, which raised the possibility that an *Lmx1b*→*Pet1* regulatory cascade acts in the formation of 5-HT axons.

To investigate this idea, we generated *Pet1*cKO (*Pet1*^{fl/fl};*Pet1-Cre*;*Ai9*) and control (*Pet1*^{+/+};*Pet1-Cre*;*Ai9*) mice (**Liu et al., 2010**). We imagined three alternative experimental outcomes: i, *Pet1*cKO fully phenocopies the axon defects found in *Lmx1b*cKO supporting an exclusive *Lmx1b*→*Pet1* regulatory cascade in 5-HT axon formation, ii, 5-HT axon projection pathways are intact in *Pet1*cKO mice and therefore the *Lmx1b*→*Pet1* regulatory path is not operational in 5-HT axon development or iii, *Pet1*cKO incompletely phenocopies *Lmx1b*cKO axon defects suggesting that the *Lmx1b*→*Pet1* cascade operates in parallel with other *Lmx1b* orchestrated regulatory programs.

We first examined TdTomato⁺ axon patterns in adult *Pet1*cKO versus control spinal cords. We confirmed *Pet1* transcript loss in medullary 5-HT neurons by in situ hybridization (ISH) (**Figure 8—figure supplement 1A**). TdTomato⁺ axon patterns from cervical to lumbar levels of the spinal cord were similar in *Pet1*cKO and control mice (**Figure 8A**). Quantitation of total TdTomato⁺ axons in gray and white matter revealed no significant difference between *Pet1*cKO and control mice (**Figure 8B**). These findings indicate that *Pet1*, and consequently the hypothetical *Lmx1b*→*Pet1* cascade, is not required for the formation of descending 5-HT axon pathways (**Figure 8—figure supplement 1E**).

We next investigated the *Pet1*cKO forebrain and found in striking contrast to the spinal cord that few if any TdTomato⁺ axons were present in the olfactory bulb, cortex, amygdala, hippocampus, striatum and many regions of the hypothalamus in *Pet1*cKO forebrains (**Figure 8C–E**). Furthermore, the pattern of TdTomato⁺ axons in the thalamus of *Pet1*cKO mice was severely disrupted with notable patches of clumped fibers and other areas with few, if any, fibers (**Figure 8—figure supplement 1B**). Similar to *Lmx1b*cKO mice, TdTomato⁺ axons were present in normal density and with proper ascending trajectory within the MFB of *Pet1*cKO mice (**Figure 8—figure supplement 1C**). These findings clearly demonstrate a requirement for *Pet1* in forebrain 5-HT pathway formation and thus distinct transcription factor requirements in the generation of ascending and descending 5-HT axon projection pathways.

Although *Pet1* conditional targeting largely phenocopies the forebrain 5-HT axon defects found in *Lmx1b*cKO mice, we noticed distinctly different patterns of TdTomato⁺ arbors in the *Pet1*cKO vs. *Lmx1b*cKO thalamus (**Figure 8—figure supplement 1B**). The *Pet1*cKO thalamus lacked TdTomato⁺ axons in lateral regions while in other thalamic regions we found abnormal clumping of *Pet1*cKO TdTomato⁺ axons (**Figure 8—figure supplement 1B**). Further, in contrast to the failure of *Lmx1b*cKO axons to demarcate the PVT, *Pet1*cKO TdTomato⁺ axons were properly patterned in this

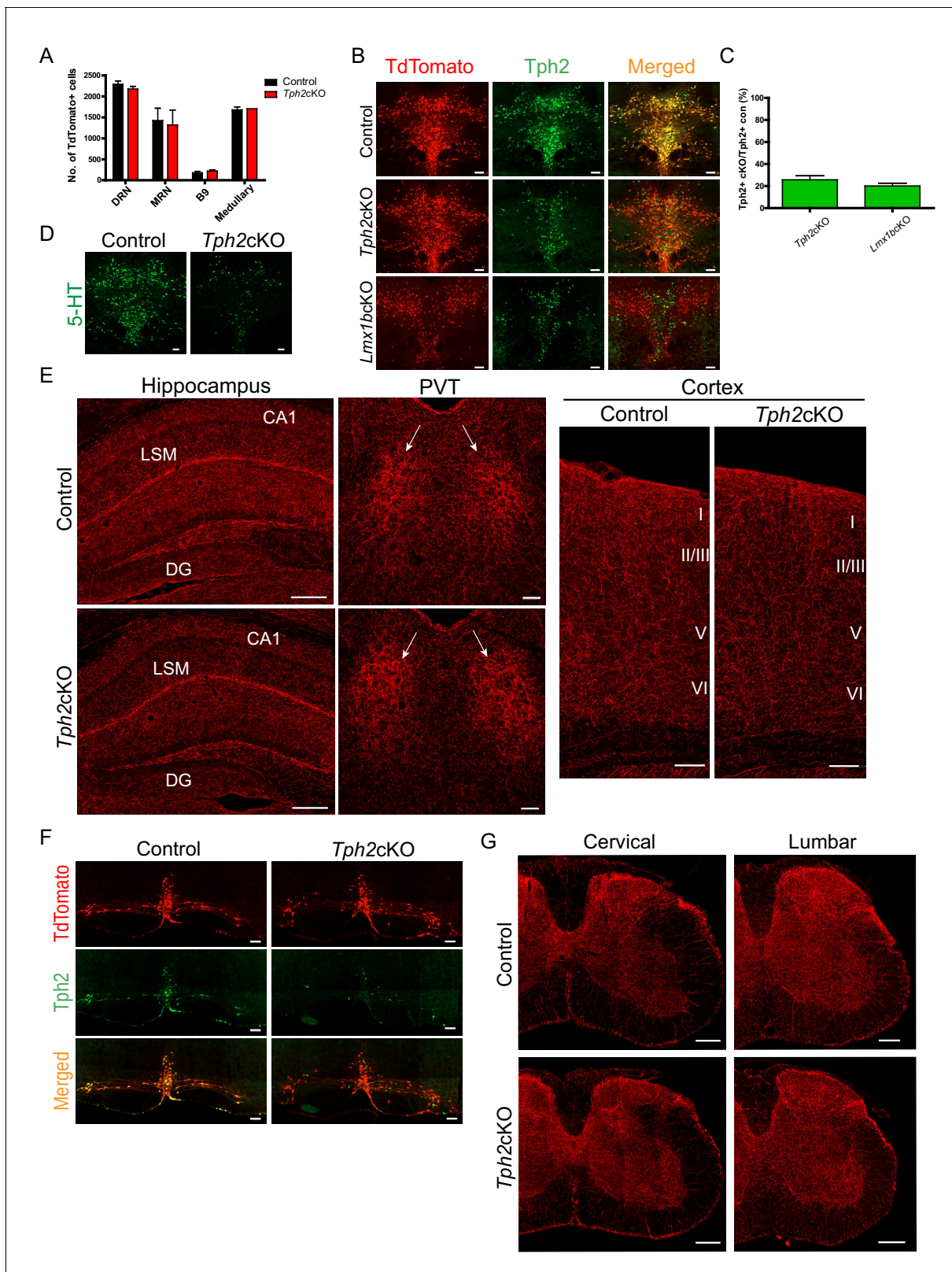


Figure 6. Specific targeting of 5-HT synthesis does not alter 5-HT arborization patterns. (A) Counts of TdTomato+ cells in each raphe nucleus of *Tph2*cKO mice did not differ from controls (n = 2 mice/genotype). Data are represented as mean ± SEM. (B) Comparable Tph2 knock-down in *Tph2*cKO and *Lmx1bc*KO mice. Scale bars, 100 μm. (C) Cell counts of residual Tph2+ neurons in *Tph2*cKO and *Lmx1bc*KO mice expressed as a percentage (n = 2 mice/genotype). Data are represented as mean ± SEM. (D) Immunolabeling shows 5-HT was severely reduced in *Tph2*cKO mice. Figure 6 continued on next page

Figure 6 continued

Scale bars, 100 μm . (E) Coronal forebrain sections showing no deficits of TdTomato⁺ axon densities in *Tph2*CKO hippocampus, PVT, and cortex ($n = 3$ mice/genotype). LSM, lacunosum moleculare; DG, dentate gyrus; CA1 of hippocampus. Scale bars, 100 μm (PVT, cortex); 200 μm (hippocampus). (F) Co-immunolabeling for Tph2 and TdTomato in medullary neurons. Tph2 expression was severely reduced in medullary neurons of *Tph2*CKO mice. Scale bars, 50 μm . (G) No deficits of TdTomato⁺ axons were present throughout the *Tph2*CKO spinal cord ($n = 3$ mice/genotype). Scale bars, 200 μm .

DOI: <https://doi.org/10.7554/eLife.48788.013>

region (**Figure 8—figure supplement 1B**). This suggests *Lmx1b* may act independently of *Pet1* in this specific highly discrete target field. Interestingly, early *Pet1* deficiency did not result in reduced cell body size thus demonstrating that reduced cell body size did not contribute to the axon defects in *Lmx1b*CKO mice (**Figure 8—figure supplement 1D**). The robust similarities and yet distinct differences in TdTomato⁺ axon patterns in *Pet1*CKO compared to *Lmx1b*CKO forebrain support a model in which *Lmx1b*→*Pet1* is the main regulatory program but that additional minor *Lmx1b*- or *Pet1*-orchestrated regulatory pathways operate in building ascending 5-HT axonal architectures (**Figure 8—figure supplement 1F**).

We investigated whether *Lmx1b* and *Pet1* compensate for one another in the formation of 5-HT axons, by examining double-targeted mice (DKO: *Lmx1b*^{fl/fl}; *Pet1*^{fl/fl;Pet1-Cre;Ai9}) and controls (*Lmx1b*^{+/+}; *Pet1*^{+/+;Pet1-Cre;Ai9}). Analysis of DKO spinal cords revealed deficits in TdTomato⁺ axon patterns to similar levels as *Lmx1b*CKO spinal cord, further confirming *Pet1* does not play a role in descending 5-HT axon development (**Figure 8—figure supplement 2A**). In the forebrain, we did not find a more extreme deficit in TdTomato⁺ axons in DKO mice compared to *Lmx1b*CKO mice. The DKO thalamus mirrored the *Lmx1b*CKO thalamus in the specific clumping of arbors and inability to properly pattern arbors in the PVT (**Figure 8—figure supplement 2B**).

To investigate whether the initial 1–2 days of *Pet1* expression, not targeted by *Pet1-Cre* in *Pet1*CKO mice is required for primary ascending pathway formation, we analyzed *Pet1*^{-/-;Pet1-YFP} mice in which the *Pet1-YFP* transgene labels control and mutant *Pet1*⁺ cell bodies and their axons with YFP (**Hawthorne et al., 2010**). We found comparable initial 5-HT primary axon outgrowth in *Pet1*^{-/-} and control 5-HT neuron cell bodies at E13.5 (**Figure 8—figure supplement 2C**).

Lmx1b acts through Pet1 to temporally control postnatal stage-specific gene expression and forebrain arborization

Stage-specific regulatory functions suggest potential stage-specific control of gene expression to fulfill successive steps in the morphological maturation of axon projection pathways. Thus, we next sought to determine whether the *Lmx1b*→*Pet1* cascade temporally regulates expression of axon-related genes that are required at specific stages of 5-HT pathway formation. We found that *Lmx1b* continues to control *Pet1* postnatally as *Pet1* transcript levels were decreased in P3 targeted *Lmx1b*CKO mice (**Figure 9A,B**). Next, we used RNA-sequencing to find common *Lmx1b* and *Pet1* targets. Comparing rostral *Lmx1b* and *Pet1* regulated genes, we found 82 regulated genes present in both datasets (**Figure 9C**). By intersecting rostral *Lmx1b* and *Pet1* regulated genes with the set of *Lmx1b*-regulated axon-related genes (**Supplementary file 1**), we found 15 co-regulated genes (**Figure 9C**). Interestingly, one of these coregulated genes is *Pcdhac2*. Extensive studies of *Pcdhac2* have demonstrated its key intrinsic role in the formation and patterning 5-HT axon arbors (**Chen et al., 2017; Katori et al., 2009; Katori et al., 2017**). In particular, *Pcdhac2* deficient mice exhibit a lack of forebrain 5-HT arbors and severe clumping of remaining arbors, thus raising a functional link to *Lmx1b* and *Pet1*.

Since *Pcdhac2* is in the *Pcdh* alpha gene cluster and shares 3 (out of 4) exons with all other *Pcdh* alpha genes, we performed differential exon expression analysis with the *Lmx1b* and *Pet1* RNA-seq datasets. By testing the only unique exon for *Pcdhac2*, we found that *Pcdhac2* was significantly regulated by *Lmx1b* and *Pet1* at E17.5 (**Figure 9D**). In contrast, *Pcdhac2* expression was not significantly regulated by *Pet1* at earlier stages (**Wyler et al., 2016**). Furthermore, our time-series RNA-seq analyses (**Wyler et al., 2016**) showed a significant and dramatic upregulation of *Pcdhac2* only at the onset of the arborization stage (**Figure 9E**). Thus, *Pcdhac2* expression is precisely controlled at the stage in which it is required for morphological maturation of 5-HT neurons.

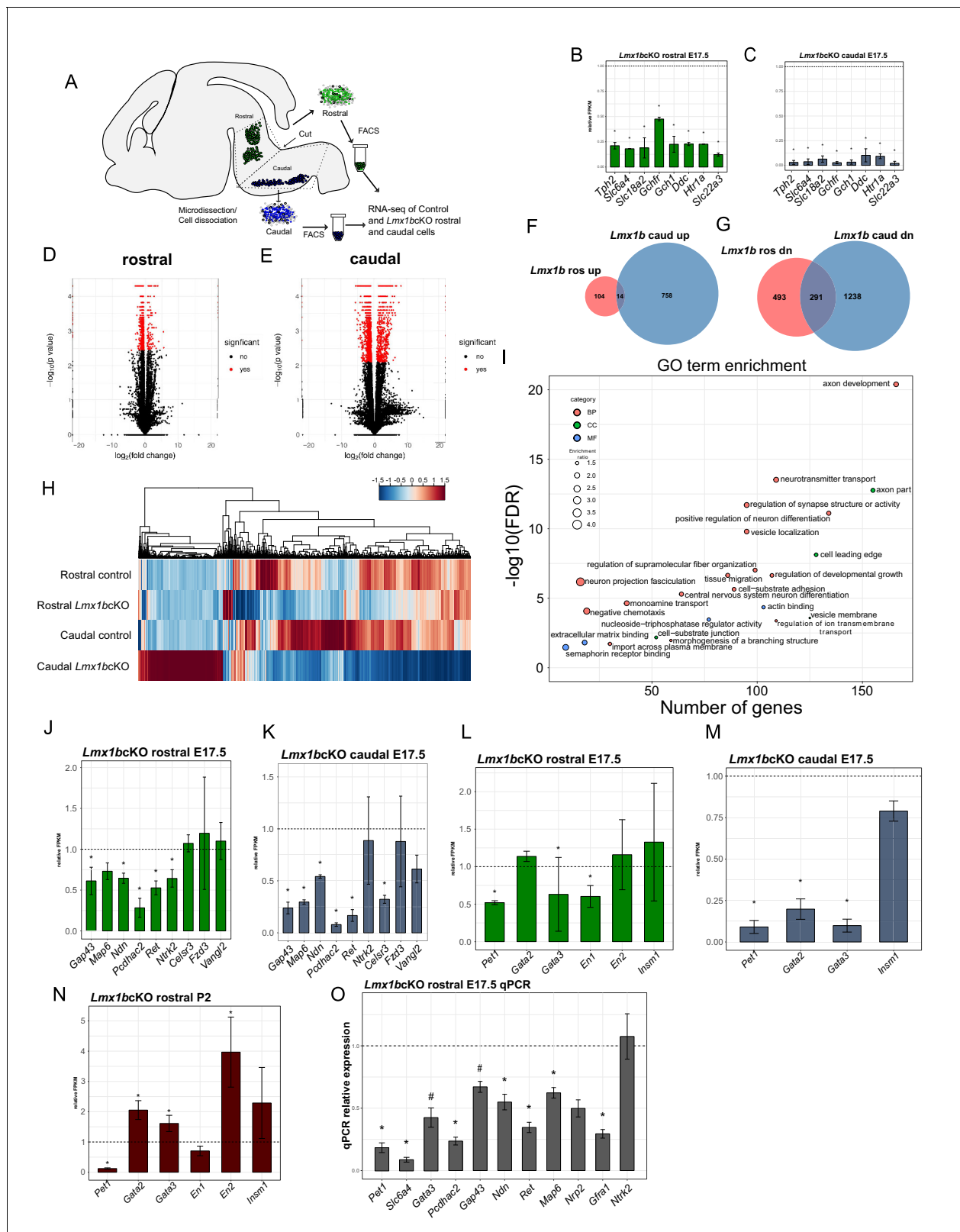


Figure 7. Ascending and descending *Lmx1b* regulated transcriptomes. (A) Schematic for dissection of E17.5 brain to isolate rostral and caudal 5-HT neurons genetically labeled by *Pet1-EYFP*. After dissection, *EYFP*⁺ neurons were flow-sorted separately and prepared for RNA-sequencing (n = 3, controls; n = 2 *Lmx1b*KO embryos). (B) Relative expression level of 5-HT pathway genes in rostral control versus *Lmx1b*KO 5-HT neurons. Control gene expression levels were normalized to one. * indicates FDR ≤ 0.05. Data are represented as mean ± SEM. (C) Relative expression level of 5-HT pathway genes in caudal control versus *Lmx1b*KO 5-HT neurons. Control gene expression levels were normalized to one. * indicates FDR ≤ 0.05. Data are represented as mean ± SEM. (D) Volcano plot of significant genes in rostral neurons. (E) Volcano plot of significant genes in caudal neurons. (F) Venn diagram of *Lmx1b* upregulated (ros up) and downregulated (ros dn) genes. (G) GO term enrichment plot. (H) Heatmap of gene expression across rostral and caudal control and *Lmx1b* KO conditions. (J) Bar graph of relative expression of *Lmx1b* KO rostral E17.5 genes. (K) Bar graph of relative expression of *Lmx1b* KO caudal E17.5 genes. (L) Bar graph of relative expression of *Lmx1b* KO rostral E17.5 genes. (M) Bar graph of relative expression of *Lmx1b* KO caudal E17.5 genes. (N) Bar graph of relative expression of *Lmx1b* KO rostral P2 genes. (O) Bar graph of qPCR relative expression of *Lmx1b* KO rostral E17.5 genes.

Figure 7 continued

pathway genes in caudal control versus *Lmx1bcKO* 5-HT neurons. Control gene expression levels were normalized to one. * indicates $FDR \leq 0.05$. Data are represented as mean \pm SEM. (D) Volcano plot for rostral control versus *Lmx1bcKO* differential expression. Significantly altered genes are in red with $\geq \log_2(1.5X)$ and $FDR \leq 0.05$. (E) Volcano plot for caudal control versus *Lmx1bcKO* differential expression. Significantly altered genes are in red with $\geq \log_2(1.5X)$ and $FDR \leq 0.05$. (F) Venn diagram of genes upregulated in rostral and caudal *Lmx1bcKO* 5-HT neurons. (G) Venn diagram of genes downregulated in rostral and caudal *Lmx1bcKO* 5-HT neurons. (H) Heatmap of differentially-expressed genes in rostral and caudal *Lmx1bcKO* 5-HT neurons. (I) GO term enrichment of *Lmx1b* regulated genes. BP = biological process, CC = cellular component, MF = molecular function. GO terms were enriched with $FDR \leq 0.05$. (J) Relative expression (FPKMs) of known 5-HT neuron axon-related genes in rostral *Lmx1bcKO* 5-HT neurons. Data are represented as mean \pm SEM. (K) Relative expression (FPKMs) of known 5-HT neuron axon-related genes in caudal *Lmx1bcKO* 5-HT neurons. Data are represented as mean \pm SEM. (L) Relative expression (FPKMs) of 5-HT GRN transcription factors in rostral *Lmx1bcKO* 5-HT neurons. Data are represented as mean \pm SEM. (M) Relative expression (FPKMs) of 5-HT GRN transcription factors in caudal *Lmx1bcKO* 5-HT neurons. Data are represented as mean \pm SEM. (N) Relative expression (FPKMs) of 5-HT GRN transcription factors in flow sorted TdTomato⁺ rostral *Lmx1bcKO* 5-HT neurons at postnatal day 2 (n = 3, controls; n = 4, *Lmx1bcKO* mice). Data are represented as mean \pm SEM. (O) RT-qPCR verification of 5-HT GRN transcription factors and known axon-related genes from flow sorted rostral YFP⁺ *Lmx1bcKO* 5-HT neurons relative to control levels (n = 4 mice/genotype). * indicates $p\text{-value} \leq 0.05$, # indicates $p < 0.1$, t-test with Welch's correction. Data are represented as mean \pm SEM.

DOI: <https://doi.org/10.7554/eLife.48788.014>

To determine whether *Lmx1b* was required to control the postnatal upregulation of *Pcdhac2*, we treated *Lmx1bicKO* mice with tamoxifen at postnatal day three and analyzed *Pcdhac2* expression by ISH at P14, when arborization is profusely developing. Indeed, we found substantially reduced expression of *Pcdhac2* in P3 *Lmx1bicKO* mice (Figure 9F). To further probe whether the *Lmx1b*→*Pet1* regulatory cascade is required for upregulation of *Pcdhac2* during arborization, we generated *Pet1icKO* (*Pet1^{fl/fl}; Tph2-CreER; Ai9*) mice. We first verified that *Pet1* was effectively targeted in P3 *Pet1icKO* mice by RT-qPCR of flow sorted TdTomato⁺ cells as well as ISH for *Pet1* (Figure 9—figure supplement 1A,B). We confirmed that similar numbers of TdTomato⁺ neurons were activated in P3 *Pet1icKO* mice (Figure 9—figure supplement 1C,D) and that long-range routes were filled compared to controls (Figure 9—figure supplement 1E). We found that *Pet1* did not regulate *Lmx1b* at this stage (Figure 9—figure supplement 1A). Interestingly, we found that *Pet1* was also required for the dramatic postnatal upregulation of *Pcdhac2* expression (Figure 9G). These findings show that the *Lmx1b*→*Pet1* regulatory cascade acts during the arborization stage to temporally control *Pcdhac2* upregulation.

To determine if *Pcdhac2* is a direct target of *Lmx1b*→*Pet1*, we analyzed our previously published ChIP-seq datasets (Wylter et al., 2016) for myc*Pet1* binding sites within the *Pcdhac2* locus. Notably, we identified only two significant myc*Pet1* ChIP-seq peaks throughout the entire 250 kb *Pcdha* locus (Figure 9H). One peak was located at the 5' end of the unique *Pcdhac2* first exon. The second peak was located precisely within the third-intronic DNase I hypersensitivity site, HS7, which marks a well characterized transcriptional enhancer known to regulate midbrain expression of the *Pcdha* gene isoform (Kehayova et al., 2011; Ribich et al., 2006) (Figure 9H). Although the myc*Pet1* peak at the TSS of *Pcdhac2* does not contain a match to the known *Pet1* binding motif, the second peak within HS7 does contain a significant match to the *Pet1* motif (Wei et al., 2010) (Figure 9I).

To determine whether *Lmx1b*→*Pet1* cascade acts postnatally to control terminal arborization we analyzed the forebrains of P3 targeted *Pet1icKO* mice. Analyses performed at P49 revealed a severe deficit of 5-HT arbors in the hippocampus and cortex of P3 targeted *Pet1icKO* mice, comparable to the deficit found in P3 targeted *Lmx1bicKO* mice (Figures 5C, 5D; Figures 9J, 9K). The timing of 5-HT terminal arborization varies widely in different regions of the early postnatal forebrain (Lidov and Molliver, 1982; Maddaloni et al., 2017). Thus, we next sought to determine whether the *Lmx1b*→*Pet1* cascade continues to control arborization in forebrain regions that are late to develop their mature axon patterns. To investigate this, we administered a single dose of tamoxifen to *Pet1icKO* pups at P5. We focused our subsequent analyses on the striatum, which is one of last regions of the forebrain to develop mature 5-HT arborization patterns (Lidov and Molliver, 1982). Interestingly, we found a notable deficit in the 5-HT arbors throughout the striatum (Figure 9L; Figure 9—figure supplement 1F). Together, our findings demonstrate that the *Lmx1b*→*Pet1* cascade operates continually over an extended postnatal period to control stage-specific gene expression and to generate both early and late 5-HT terminal arbors patterns in different forebrain regions.

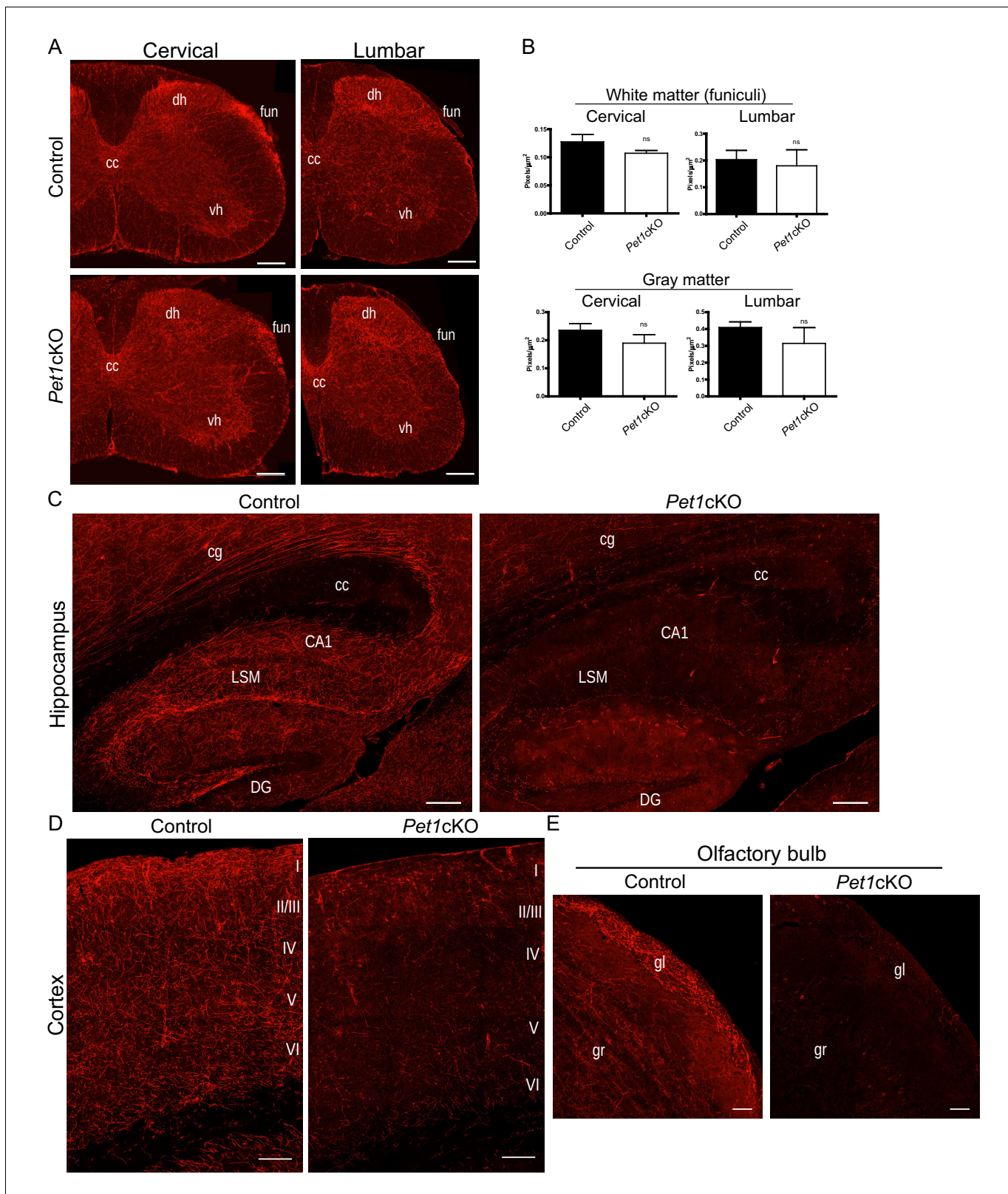


Figure 8. Distinct transcription factor requirements in the formation of ascending and descending 5-HT projection pathways. (A) TdTomato⁺ axon innervation in *Pet1cKO* vs control spinal cords in 3 month old mice. Coronal semi-section views of cervical and lumbar levels. Scale bars, 200 μm. cc, central canal; dh, dorsal horn; vh, ventral horn; fun, funiculi. (B) Quantification of TdTomato⁺ axons (pixels/μm²) in cervical and lumbar spinal cords (n = 3, controls; n = 3, *Pet1cKO* animals; Two-way ANOVA; white matter: cervical p=0.1372; lumbar p=0.6764; gray matter: cervical p=0.4440; lumbar p=0.6764). (C) Hippocampus. (D) Cortex. (E) Olfactory bulb. Figure 8 continued on next page

Figure 8 continued

$p=0.1995$). Data are represented as mean \pm SEM. (C) Decreased TdTomato⁺ arbors detected in *Pet1cKO* hippocampus compared to controls at 3 months of age. Scale bars, 200 μ m, sagittal view. (D) Decreased TdTomato⁺ arbors detected in *Pet1cKO* cortex compared to controls at 3 months of age. Scale bars, 100 μ m, coronal view. (E) Decreased TdTomato⁺ arbors detected in *Pet1cKO* olfactory bulb compared to controls at 3 months of age. Scale bars, 50 μ m, sagittal view. cg, cingulum; cc, corpus callosum; LSM, lacunosum moleculare; DG, dentate gyrus; CA1 of hippocampus; gr, granule layer; gl, glomerular layer.

DOI: <https://doi.org/10.7554/eLife.48788.015>

The following figure supplements are available for figure 8:

Figure supplement 1. *Pet1cKO* and *Lmx1bcKO* mice exhibit distinct axon defects in thalamus.

DOI: <https://doi.org/10.7554/eLife.48788.016>

Figure supplement 2. DKO and *Pet1^{-/-}* analyses.

DOI: <https://doi.org/10.7554/eLife.48788.017>

Discussion

The process of long-range axon pathway formation occurs in temporally defined stages over an extended period during which successive morphological events occur (Fame et al., 2011; Lidov and Molliver, 1982; Shirasaki and Pfaff, 2002). Many regulatory factors have been implicated in the intrinsic control (Santiago and Bashaw, 2014) of axon outgrowth, target selection, and terminal arborization (Arlotta et al., 2005; Chen et al., 2005; Galazo et al., 2016; Livet et al., 2002; Srivatsa et al., 2015). What is not understood are the intrinsic programs that operate temporally to progressively control the prolonged, multistage process of long-range axon projection pathway formation (Paolino et al., 2018). Our findings uncover a temporal regulatory strategy through which a continuously expressed transcription factor, *Lmx1b*, operates at successive stages to control progressive steps in the postmitotic morphological maturation of long-range highly diffuse axonal projection pathways. Thus, *Lmx1b* through its continuous expression not only controls the capacity for 5-HT synthesis and reuptake (Zhao et al., 2006), but also the formation of long range profusely arborized projection pathways that enable delivery of the transmitter throughout the CNS.

Our findings suggest *Lmx1b* acts to successively control 5-HT axon primary outgrowth, selective routing, and terminal arborization. We uncovered a delay in primary 5-HT axon outgrowth between E16.5 to E18.5 in *Lmx1bcKO* mice. However, initiation of primary axon outgrowth toward the forebrain or spinal cord was not disrupted in either *Lmx1bcKO*, *Pet1cKO*, or *Pet1^{-/-}* mice. As 5-HT axonogenesis occurs concomitant with the onset of 5-HT synthesis in newborn 5-HT neurons (Hawthorne et al., 2010), perhaps upstream regulatory programs operating at the progenitor stage control initial axon outgrowth from newborn 5-HT neurons (Briscoe et al., 1999; Jacob et al., 2007; Pattyn et al., 2004).

The profound defect in the subsequent selective 5-HT axon routing through the cingulum, SCS, and fornix suggests a failure of intrinsic growth extension beyond selective routing choice points. In support of this, we never observed ectopic 5-HT axon trajectories. Yet, we leave open the possibility that axon guidance defects contribute to the failure of 5-HT axons to selectively extend through proper routes. 5-HT axons normally turn dorsally through the septal area at E18.5, which might constitute a critical choice point in building expansive axon 5-HT architectures. In contrast, the vast majority of mutant 5-HT axons fail to make the dorsal turn and then fail to continue into selective tracts. In support of a possible guidance defect, our RNA-seq studies indicated that *Lmx1b* controls expression of a large number of genes encoding guidance receptors, guidance receptor ligands, and adhesion molecules.

Transcription factors function within GRNs as elucidated in the specification and differentiation of various types of neurons (Deneris and Gaspar, 2018; Guillemot, 2007; Shirasaki and Pfaff, 2002). How transcription factors temporally interact within networks to progressively generate precise connectivity patterns is poorly understood (Paolino et al., 2018). A focus of our experiments was to determine whether *Lmx1b* functions in the context of the 5-HT GRN to control progressive development of 5-HT axonal pathways. We uncovered a temporal requirement for *Lmx1b* in maintaining *Pet1* expression during the early postnatal stage of 5-HT pathway formation. This finding together with postnatal temporal targeting of *Pet1* revealed the *Lmx1b*→*Pet1* regulatory cascade acts stage specifically to control selective pathway routing and arborization of forebrain 5-HT axons. Despite

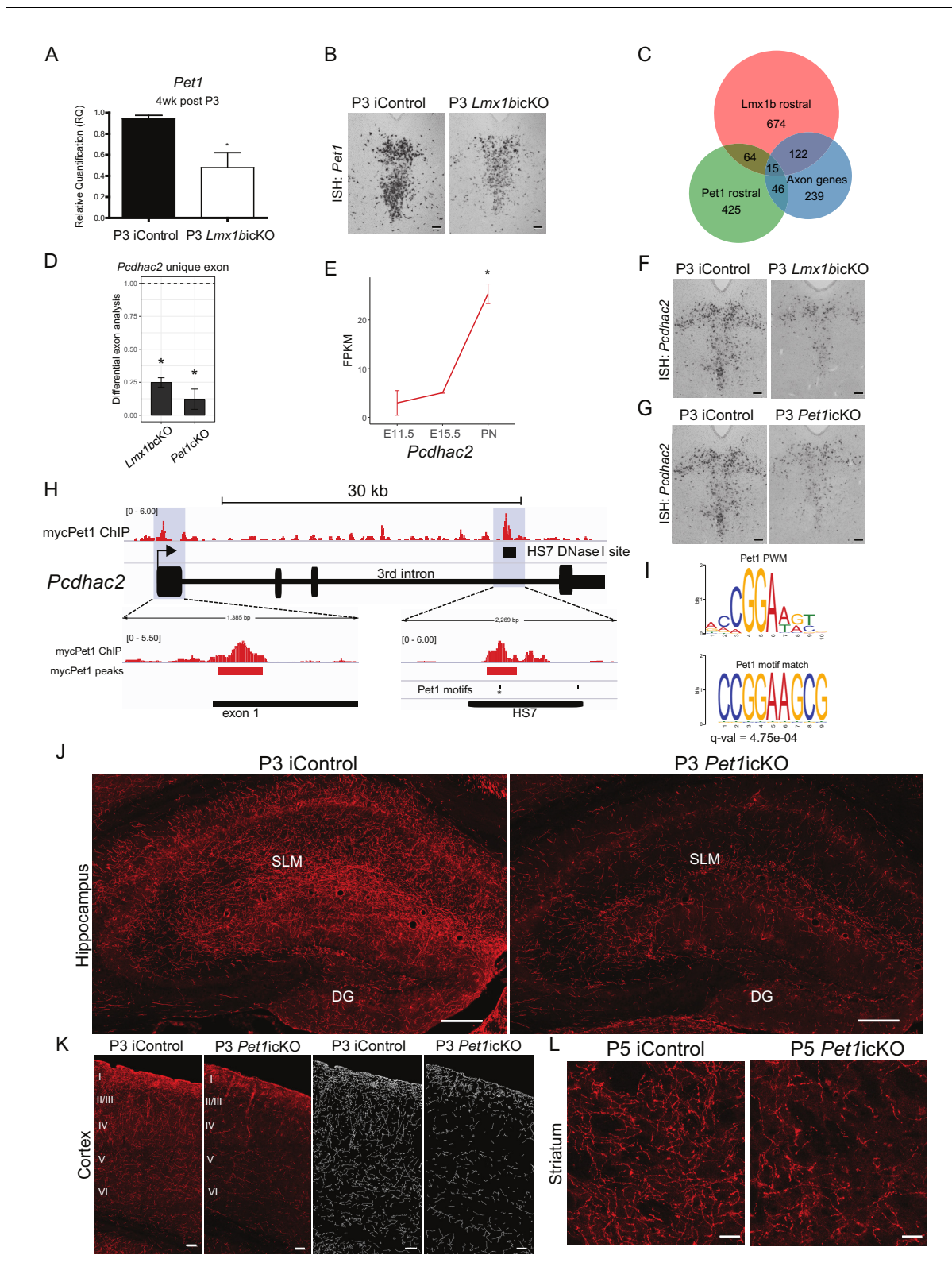


Figure 9. An ascending specific *Lmx1b*→*Pet1* cascade controls stage specific 5-HT gene expression and postnatal terminal arborization. (A) RT-qPCR analysis of *Pet1* expression in flow sorted TdTomato⁺ neurons 4 weeks post P3 tamoxifen treatment (n = 3, iControl; n = 4, P3 *Lmx1bicKO* mice). Unpaired t-test with Welch’s correction, *p<0.05. Data are represented as mean ± SEM. (B) *Pet1* in situ hybridization in P3 targeted *Lmx1bicKO* mice. Scale bars, 100 μm. (C) Venn diagram showing overlap of rostral *Lmx1b* and *Pet1* regulated genes and the axon-related gene dataset. *Lmx1b* Figure 9 continued on next page

Figure 9 continued

rostral: genes controlled by Lmx1b in rostral 5-HT neurons; Pet1 rostral: genes controlled by Pet1 in rostral 5-HT neurons; Axon genes: Lmx1b regulated rostral and caudal axon-related genes. (D) Relative expression of the unique *Pcdhac2* exon in rostral *Lmx1bcKO* and *Pet1cKO* 5-HT neurons. * indicates $FDR \leq 0.05$. Data are represented as mean \pm SEM. (E) Developmental expression profile of *Pcdhac2* in 5-HT neurons from E11.5 to early postnatal (PN). * indicates $FDR \leq 0.05$. Data are represented as mean \pm SEM. (F) *Pcdhac2* in situ hybridization at postnatal day 14 in P3 targeted *Lmx1bcKO* mice. Representative image from $n = 3$ mice/genotype. Scale bars, 100 μm . (G) *Pcdhac2* in situ hybridization at postnatal day 14 in P3 targeted *Pet1cKO* mice. *ISH* experiments done in parallel, iControl section is the same section in (F) and (G) to compare iCKOs at the same tissue level. Representative image from $n = 3$ *Pet1cKO* mice. Scale bars, 100 μm . (H) Visualization of the *Pcdhac2* gene locus showing mycPet1 ChIP peaks at the TSS and 3rd intron (shaded) and matches to the known Pet1 motif. Zoomed regions of the significant mycPet1 binding sites are shown at the bottom. (I) The mycPet1 binding region located within the 3rd *Pcdhac2* intron DNase I hypersensitivity site (HS7) contains a significant match to the known Pet1 position-weight matrix. TOMTOM q-value = 4.75×10^{-04} . (J) Decreased TdTomato⁺ arbors detected in P3 targeted *Pet1cKO* hippocampus compared to iControl mice. Scale bars, 200 μm . (K) Decreased TdTomato⁺ arbors detected in all layers of P3 targeted *Pet1cKO* cortex (Imaris tracing; right panels) compared to iControl mice. Scale bars, 50 μm . (L) Decreased TdTomato⁺ arbors in striatum of P5 targeted *Pet1cKO* mice. Scale bars, 20 μm . See also **Figure 9—figure supplement 1F**.

DOI: <https://doi.org/10.7554/eLife.48788.018>

The following figure supplement is available for figure 9:

Figure supplement 1. Lmx1b→Pet1 cascade acts postnatally to control 5-HT terminal arborization.

DOI: <https://doi.org/10.7554/eLife.48788.019>

the requirement for Pet1 in the acquisition of medullary 5-HT neuron-type identity (**Hendricks et al., 2003; Kiyasova et al., 2011**), it was surprising to find that Pet1 was not required for routing and arborization of descending 5-HT axons, thus revealing distinct transcription factor requirements in the generation of ascending and descending 5-HT axon pathways. Perhaps, Lmx1b operates with other continuously expressed serotonergic transcription factors in a regulatory cascade to control descending 5-HT axonal pathways. Gata3 is an interesting candidate as it functions more prominently in the medullary 5-HT neurons that generate the descending subsystem than 5-HT neurons that give rise to the ascending subsystem (**Pattyn et al., 2004; van Doorninck et al., 1999**).

The hundreds of axon related genes controlled by Lmx1b in the ascending and descending subsystems suggests that mis-expression of scores of functionally diverse effector genes accounts for the axon pathway defects we have reported. One gene of note is *Gap43*. Telencephalic commissures of *Gap43* null mice fail to form, including the hippocampal commissure and the corpus callosum (**Shen et al., 2002**). This may largely explain the 5-HT neuron axonal projection deficits reported in the *Gap43* null forebrain (**Donovan et al., 2002**). Although *Gap43* is expressed in 5-HT neurons, it is not yet known whether it plays an intrinsic role in 5-HT axon development (**Bendotti et al., 1991**). Our findings highlight the potential importance of an intrinsic Lmx1b→Pet1→*Gap43*→5-HT axon regulatory path given that *Gap43* expression is reduced in both *Lmx1bcKO* and *Pet1cKO* mice. It will be interesting to investigate this putative path in 5-HT conditionally targeted *Gap43* mice to determine whether it accounts for the selective routing defects present in *Lmx1bcKO* and *Pet1cKO* mice.

The stage specific regulatory roles we have uncovered suggests Lmx1b may temporally control certain genes to fulfill stage-specific events in the morphological maturation of 5-HT neurons. In support of this idea, our findings reveal that *Pcdhac2*, a key intrinsic effector of 5-HT terminal arbor growth and patterning (**Chen et al., 2017; Katori et al., 2009; Katori et al., 2017**), is dynamically regulated by the ascending Lmx1b→Pet1 cascade. Tamoxifen-inducible targeting of Lmx1b and Pet1 revealed a temporal requirement for Lmx1b and Pet1 in the postnatal upregulation of *Pcdhac2*. Notably, our ChIP-seq datasets revealed Pet1 occupancy at the *Pcdhac2*-specific promoter and HS7 suggesting Lmx1b→Pet1 directly controls upregulation of *Pcdhac2* during the postnatal arborization stage. Perhaps Pet1 occupancy at HS7 facilitates cohesin-mediated looping from HS7 to the *Pcdhac2* promoter thus accounting for Pet1 occupancy at this promoter in the absence of a high affinity Pet1 binding motif (**Guo et al., 2012**).

Deficient expression of a single stage-specifically expressed target gene such as *Pcdhac2* likely does not account for the severe and complex multi-stage defects in long-range 5-HT axon pathway formation reported here. However, our studies do serve to illustrate the concept that Lmx1b and Pet1 are critical terminal selectors of neuronal morphology and likely do so by dynamically regulating downstream genes that are required at specific stages for the progressive morphological maturation

of 5-HT neurons. Perhaps subsets of *Lmx1b* controlled genes act in different 5-HT neuron subtypes and at distinct stages to control the specific routes of 5-HT axons to diverse forebrain and spinal cord targets.

We speculate that our findings illustrate a possible general mechanism through which continuously expressed terminal selectors build long-range diffuse axon pathways. In addition to 5-HT neurons, noradrenergic, dopaminergic, and histaminergic neurons also generate expansive and highly arborized axonal architectures (Björklund and Dunnett, 2007; Haas et al., 2008; Moore and Bloom, 1979). *Lmx1b* plays a critical role in dopaminergic (DA) neuron development. However, in contrast to 5-HT neurons, *Lmx1b* is co-expressed in postmitotic DA neurons with its paralog, *Lmx1a*, up to about 2 months of age (Laguna et al., 2015). These two LIM HD factors play compensatory roles in mesDA neuron specification and differentiation (Laguna et al., 2015; Yan et al., 2011). Simultaneous DA targeting of *Lmx1a* and *Lmx1b* beginning at E14 resulted in diminished DA axon outgrowth to the dorsal striatum while DA axon projections to the ventral striatum and other DA axon targets throughout the forebrain remained intact (Chabrat et al., 2017). These findings suggest that temporal control of axon routing and arborization of the DA mesostriatal, mesolimbic and mesocortical projection pathways may be controlled by different continuously acting terminal selector transcription factors expressed in DA neurons.

In addition to their tremendous intrinsic capacity for long-range axonal growth and arborization during development, 5-HT neurons are noted for their rare ability to sprout and regenerate axons after injury (Hawthorne et al., 2011; Jin et al., 2016). Given *Lmx1b*'s continuous expression into adulthood and crucial function in the formation of 5-HT projection pathways an intriguing line of investigation will be to determine whether *Lmx1b* transcriptionally powers 5-HT neuron's intrinsic potential for axon regrowth following injury in adult brain or spinal cord, which may suggest ways to harness that power for development of new repair strategies.

Materials and methods

Key resources table

Reagent type (species) or resource	Designation	Source or reference	Identifiers	Additional information
Gene (<i>Mus musculus</i>)	<i>Lmx1b</i>	NA	MGI:1100513	
Gene (<i>M. musculus</i>)	<i>Pet1</i>	NA	MGI:2449712	
Gene (<i>M. musculus</i>)	<i>Tph2</i>	NA	MGI:2651811	
Genetic reagent (<i>M. musculus</i>)	<i>Pet1-Cre</i>	PMID:16251278	RRID:MGI:4837211	Evan Deneris (Case Western Reserve University)
Genetic reagent (<i>M. musculus</i>)	<i>RosaTom</i>	Jackson Laboratory	Stock #: 007909; RRID:MGI:4436851	Hongkui Zeng (Allen Institute for Brain Science)
Genetic reagent (<i>M. musculus</i>)	<i>Tph2-CreERT2</i>	Jackson Laboratory	Stock #: 016584; RRID:IMSR_JAX:016584	Bernd Gloss (NIEHS)
Genetic reagent (<i>M. musculus</i>)	<i>Lmx1bflox</i>	PMID:17151281	RRID:MGI:3810753	Zhou-Feng Chen (Washington University)
Genetic reagent (<i>M. musculus</i>)	<i>Pet1flox</i>	PMID:20818386	RRID:MGI:4837213	Evan Deneris (Case Western Reserve University)
Genetic reagent (<i>M. musculus</i>)	<i>Tph2flox</i>	PMID:24972638	RRID:IMSR_JAX:027590	Zhou-Feng Chen (Washington University)

Continued on next page

Continued

Reagent type (species) or resource	Designation	Source or reference	Identifiers	Additional information
Genetic reagent (<i>M. musculus</i>)	<i>Pet1</i> ^{-/-}	PMID:12546819	MGI:2449922	Evan Deneris (Case Western Reserve University)
Genetic reagent (<i>M. musculus</i>)	<i>Pet1</i> -YFP	PMID:16251278	n/a	Evan Deneris (Case Western Reserve University)
Antibody	anti-RFP (rabbit polyclonal)	Rockland	Rockland: p/n 600-401-379; RRID:AB_2209751	(1:200)
Antibody	anti-GFP (rabbit polyclonal)	Invitrogen	Invitrogen: A6455; RRID:AB_221570	(1:200)
Antibody	anti-5-HT (rabbit polyclonal)	Immunostar	Immunostar: 20080; RRID:AB_1624670	(1:200)
Antibody	anti-Tph2 (rabbit polyclonal)	Millipore	Millipore: ABN60; RRID:AB_10806898	(1:500)
Antibody	anti-Lmx1b (rabbit polyclonal)	<i>Suleiman et al., 2007</i> -gift	n/a	(1:200)
Antibody	anti-RFP (mouse monoclonal)	Abcam	Abcam: ab65856; RRID:AB_1141717	(1:200)
Antibody	anti-RFP (mouse monoclonal)	Rockland	Rockland: p/n 200-301-379; RRID:AB_2611063	(1:200)
Antibody	Alexa 488- or 594-secondaries	Invitrogen		(1:500)
Genetic reagent (Virus)	rAAV2/Ef1a-DIO-hchr2 (H134R)-EYFP	UNC GTC Vector Core		Lot# AV4378K
Sequence-based reagent	<i>Pcdhac2</i> in situ primer: F: 5' AGCCACCTCTAT CAGCTACCG 3'	this paper		
Sequence-based reagent	<i>Pcdhac2</i> in situ primer: R: 5' AGAATTAACC CTCACTAAAGGGCTCAT TTTGAGAGCCAGCATCA 3'	this paper		
Sequence-based reagent	<i>Pet1</i> in situ primers: F:5'CCAGTGACCA ATCCCATCCTC3'	PMID:26843655		
Commercial assay or kit	Transcriptor First Strand cDNA Synthesis Kit	Roche	REF 4896866001	
Commercial assay or kit	PerfeCTa PreAmp SuperMix	QuantoBio	Cat. No. 95146-040	
Commercial assay or kit	PerfeCTa FastMix II ROX mastermix	QuantaBio	Cat. No. 95119-012	
Commercial assay or kit	RNA Clean and ConcentratorTM-5 kit	Zymo Research	Catalog Nos. R1015 and R1016	
Chemical compound, drug	Tamoxifen	Sigma-Aldrich	CAS Number: 10540-29-1	10 mg/mL stock in corn oil
Other	35 µm filter	BD biosciences	Cat. No. 352235	
Other	Fetal bovine serum (FBS)	Gibco	Cat. No. 16000044	
Other	DNase I	Invitrogen	Cat. No. 18047019	
Other	Trizol LS	Invitrogen	Cat. No. 10296010	

Continued on next page

Continued

Reagent type (species) or resource	Designation	Source or reference	Identifiers	Additional information
Other	TrypLE	Invitrogen	Cat. No. 12605010	
Other	Leibovitz's L15 medium	Invitrogen	Cat. No. 11415114	
Commercial assay or kit	Quantifluor RNA system	Promega	Cat. No. E3310	
Commercial assay or kit	Nugen TRIO RNA-seq	Nugen	Cat. No. 0507–08	
Commercial assay or kit	Zymo RNA clean and concentrator	Zymo Research	Cat. No. R1013	
Other	FACS Aria I	Becton Dickinson		
Other	iCyt cell sorter	Sony		
Other	Fragment analyzer	Advanced Analytics		
Other	Nextseq 550	Illumina	RRID:SCR_016381	
Software, algorithm	FASTQC	https://www.bioinformatics.babraham.ac.uk/projects/fastqc/	RRID:SCR_014583	
Software, algorithm	Trimmomatic	Bolger et al., 2014	RRID:SCR_011848	
Software, algorithm	Cufflinks (v2.2.2)	Trapnell et al., 2010	RRID:SCR_014597	
Software, algorithm	R (v. 3.5)	http://www.r-project.org	RRID:SCR_001905	
Software, algorithm	Webgestalt	http://www.webgestalt.org	RRID:SCR_006786	
Software, algorithm	Bioenn	http://www.bioenn.nl		
Software, algorithm	DEXSeq	Anders et al., 2012	RRID:SCR_012823	
Software, algorithm	Tophat2 (v2.1.1)	Kim et al., 2013	RRID:SCR_013035	
Other	<i>Mus musculus</i> genome	Ensembl, v. 96	RRID:SCR_002344	
Other	<i>Mus musculus</i> genome	UCSC, mm10	RRID:SCR_005780	
Software, algorithm	featureCounts	Rsubread	RRID:SCR_012919	
Software, algorithm	ENCODE Transcription Factor ChIP-seq analysis pipeline	https://github.com/ENCODE-DCC/chip-seq-pipeline	RRID:SCR_015482	
Software, algorithm	Burroughs-Wheeler aligner (BWA)	http://bio-bwa.sourceforge.net/	RRID:SCR_010910	
Software, algorithm	MACS2	Zhang et al., 2008	RRID:SCR_013291	
Software, algorithm	Imaris 7.4.2	Bitplane, Zurich, Switzerland	Surfaces or Filament Tracer tool	

Animals

All procedures were approved by the Institutional Animal Care and Use Committees of Case Western Reserve University in accordance with the National Institutes of Health Guide for the *Care and Use of Laboratory Animals*. Experiments were performed on male and female mice using age-matched and sex-matched controls in triplicate unless otherwise noted. Adult mice between the ages 2.5 to 3.5 months were used unless otherwise noted. Early conditional knockout mice (designated *Lmx1bcKO*, *Pet1cKO*, and *Tph2cKO*) were generated by using the following genetic mouse lines: *Pet1-Cre* (original name *ePet-Cre*) (**Scott et al., 2005**), *Ai9 Rosa TdTomato* (*Rosa^{Tom}*; Jackson labs) and either *Lmx1b^{fl}* (**Zhao et al., 2006**), *Pet1^{fl}* (**Liu et al., 2010**), or *Tph2^{fl}* (**Kim et al., 2014**). All early conditional knockout mice were compared to non-floxed controls (+/+; *Pet1-Cre*;*Ai9*). The following genetic lines were used to generate *Lmx1bcKO* or *Pet1cKO* mice for postnatal stage conditional knockout: *Tph2-Cre^{ERT2}* (Jackson lab), *Ai9 Rosa TdTomato* (*Rosa^{Tom}*; Jackson lab) and either *Lmx1b^{fl}* (**Zhao et al., 2006**) or *Pet1^{fl}* (**Liu et al., 2010**). All postnatal stage

conditional knockout mice were compared to non-floxed controls (iControls: +/+; *Tph2-CreER*; Ai9). *Pet1*^{-/-} mice (Hendricks et al., 2003) carrying the *Pet1-YFP* transgene (Scott et al., 2005) were used for embryo studies at E13.5. Tail or ear genomic DNA was used to determine genotypes of all animals. All mice were housed in ventilated cages on a 12 hr light/dark cycles with access to food and water with 2–5 mice per cage.

Embryos and postnatal pups

All embryo experiments at each time point were performed in triplicate unless otherwise noted and compared to littermate controls (*Lmx1b*^{fl/+} vs *Lmx1b*^{fl/fl}; *Pet1*^{fl/+} vs *Pet1*^{fl/fl}; *Pet1*^{+/-} vs *Pet1*^{-/-}). Both male and female littermates were used for analysis. Embryonic day 0.5 (E0.5) was determined by presence of a vaginal plug. Postnatal day 0 (P0) was designated by date of birth.

Histology and immunohistochemistry

Adult mice were anesthetized with Avertin (44 mM tribromoethanol, 2.5% tert-amyl alcohol, 0.02 ml/g body weight) and perfused for 2–3 min with cold PBS followed by 20 min cold 4% paraformaldehyde (PFA) in PBS. Brains and/or spinal cords were removed, post-fixed in 4%PFA for 2 hr and placed in 30% sucrose/PBS overnight (O/N) for cryoprotection. E12-E13 embryos were drop fixed in 4% PFA in PBS O/N followed by 30% sucrose incubation O/N. All embryos between age E15-E18 were transcardially perfused with 5 mL of 4% PFA in PBS, incubated in 4% PFA in PBS O/N, and incubated in 30% sucrose O/N. All tissue collected was frozen in Optimal Cutting Temperature (OCT) solution and sectioned on a cryostat at 25 μ m. Tissue sections were mounted on SuperFrost Plus slides (Thermo Fisher Scientific) and vacuum dried. Sections were then permeabilized in 0.3% Triton 100X-PBS (PBS-T) for 15 min followed by antigen retrieval in Sodium Citrate buffer for 5 min in the microwave at low power. Sections were blocked with 10% NGS in PBS-T for 1 hr followed by incubation in primary antibody using a rabbit anti-RFP antibody (1:200; p/n 600-401-379, Rockland) at 4 °C O/N. Antigen retrieval step was not used for the following primary antibodies: rabbit anti-GFP (1:200; A6455, Invitrogen), rabbit anti-5-HT (1:200; Immunostar), rabbit anti-Tph2 (1:500; ABN60, Millipore), and rabbit anti-Lmx1b (1:200; Suleiman et al., 2007). For all co-stains with TdTomato a mouse anti-RFP (1:200; ab65856, Abcam) or a mouse anti-RFP (1:200; p/n 200-301-379, Rockland) primary antibody was used. Secondary antibodies were used at 1:500; goat anti-rabbit or mouse, Alexa Fluor 594 or 488 (Invitrogen).

In situ hybridization

In situ hybridization was performed using a standard protocol using a digoxigenin-11-UTP labeled antisense RNA probe to detect *Pet1* and *Pcdhac2* (Roche diagnostics) as described elsewhere (Wyler et al., 2016). *Pcdhac2* probe (566 bp) was generated using the following primers: F: 5' AGC-CACCTCTATCAGCTACCG 3' and R: 5' AGAATTAACCCTCACTAAAGGGCTCATTTTGAGAGC-CAGCATCA 3'. *Pet1* probe (513 bp) was generated using primers: F:5'CCAGTGACCAATCCCATCC TC3' and R: 5'AGAATTAACCCTCACTAAAGGGTAAATGGGGCTGAAAGGGATA3'.

Cell counts

5-HT neurons were identified by Tph2 immunostaining. To calculate the *Pet1-Cre* efficiency, every 4th section was taken through the entire rostrocaudal extent of the DRN/MRN/B9 and medullary areas of control mice (n = 2 control mice) and RFP⁺/TPH2⁺ and TPH2⁺/RFP⁺ ratios were calculated. *Tph2-CreER* efficiency in postnatal tamoxifen injected pups was calculated from sections taken through the entire rostrocaudal extent of the DRN/MRN/B9 and expressed as a ratio of RFP⁺/TPH2⁺ and TPH2⁺/RFP⁺ cells (n = 4 iControl mice). A computer program that permits blinded manual cell counting was used (Fox and Deneris, 2012) to determine numbers of TdTomato⁺ cells between control vs *Lmx1bcKO*, control vs *Tph2cKO*, and iControl vs *Lmx1bicKO* or *Pet1icKO* mice. Every 4th matched section was counted through the entire rostrocaudal extent of the DRN/MRN/B9 or medullary 5-HT system as described. To calculate the percentage of remaining Tph2⁺ neurons in *Lmx1bcKO* vs *Tph2cKO* mice, Tph2⁺ neurons were counted in every 4th section throughout the DRN/MRN/B9. Tph2⁺ cell numbers in cKO animals was normalized to the number of Tph2⁺ cells in control matched sections and expressed as a percentage for each genotype comparison.

Tamoxifen injections

P1 pups ($Lmx1b^{fl/fl;Tph2-CreER;Ai9}$ and iControls; $n = 4$ mice/genotype) were injected 1X with 100 μg of tamoxifen (10 mg/mL stock in corn oil). P3 or P5 pups (P3: $Lmx1b^{fl/fl;Tph2-CreER;Ai9}$, $Pet1^{fl/fl;Tph2-CreER;Ai9}$, and iControls; $n = 3$ mice/genotype; P5: $Pet1^{fl/fl;Tph2-CreER;Ai9}$ and iControls, $n = 2$ mice/genotype) were injected 1X with 200 μg tamoxifen. All tamoxifen injections were performed subcutaneously at the back of the neck using a 30-gauge needle on a 1 mL syringe. Pups were allowed to sit for a few minutes before returning to mother. Injected mice were taken at either 31 or 49 days of age for analysis as indicated.

Viral injections

Adult animals ($Lmx1b^{fl/fl;Pet1-Cre;Ai9}$ and $Lmx1b^{+/-;Pet1-Cre;Ai9}$; $n = 2$ mice/genotype) were anesthetized with Isoflurane and stereotaxically injected unilaterally at two sites with 1.5 μL and 1 μL rAAV2/Ef1a-DIO-hchr2 (H134R)-EYFP (UNC GTC Vector Core Lot# AV4378K) at $X = 0.6$ mm, $Y = -4.2$ mm, $Z = -3.2$ mm and $X = 0.6$ mm, $Y = -4.2$ mm, $Z = -4.2$ mm relative to Bregma respectively. Animals were treated with a local anesthetic (bupivacaine HCL; Hospira) administered subcutaneously prior to surgery and with analgesic (carprofen 5 mg/Kg; Pfizer) for 3 days following. Holes were drilled through the skull to expose brain, following which a Hamilton syringe was slowly lowered to desired coordinates. Infusion rate was set to 0.1 $\mu\text{L}/\text{min}$ with 10 min after each injection to allow diffusion of virus. Animals were returned to group housing following recovery and sacrificed 10 weeks after surgery.

5-HT neuron dissociation and flow cytometry

For RNAseq analyses rostral and caudal E17.5 YFP⁺ 5-HT neurons were collected from $Lmx1b^{fl/fl;Pet1-EYFP}$ or $Pet1^{fl/fl;Pet1-EYFP}$ (controls) and $Lmx1b^{fl/fl;Pet1-EYFP;Pet1-Cre}$ or $Pet1^{fl/fl;Pet1-EYFP;Pet1-Cre}$ ($Lmx1b\text{cKO}$ or $Pet1\text{cKO}$) mice using flow cytometry. To dissociate embryonic 5-HT neurons, hindbrains were initially dissected to separate rostral 5-HT neurons from caudal 5-HT neurons in cold PBS. Tissue was transferred to 1.5 mL ependorf tubes and centrifuged at 1500 rpm for 1 min at 4 °C. PBS was removed and 500 μL 1X TrypLE Express (Gibco) was added to the tissue and incubated at 37 °C for 15 min followed by addition of L-15 media (Gibco). Samples were centrifuged for 1 min at 1500 rpm and washed 3X with PBS. Tissue was then resuspended in 500 μL L15/0.1%BSA/DNase solution and slowly triturated 30X with fire-polished Pasteur pipettes of decreasing bore size until fully suspended. Samples were then filtered, and flow sorted on a FACS Aria I or Sony iCyt cell sorter.

Postnatal 5-HT neuron dissociation was performed in either P2 $Lmx1b\text{cKO}$ or 4 week old $Lmx1b\text{cKO}$ or $Pet1\text{cKO}$ mice. Brains were sliced at 400 μm on a vibratome (Pelco easiSlicer) in continuously bubbling (95% O_2 ; 5% CO_2) aCSF solution (3.5 mM KCl, 126 mM NaCl, 20 mM NaHCO_3 , 20 mM Dextrose, 1.25 mM NaH_2PO_4 , 2 mM CaCl_2 , 2 mM MgCl_2 , 50 μM AP-V (Tocris), 20 μM DNOX (Sigma), and 100 nM TTX (Abcam)). Sections containing rostral 5-HT neurons were incubated in 1 mg/mL Protease from *Streptomyces griseus* (Sigma; P8811) in bubbling aCSF solution for 30min (P2 mice) or 45min (4-week-old mice) at room temperature. Slices were then incubated for 15min in bubbling aCSF alone at RT. TdTomato⁺ neurons were microdissected from slices in cold aCSF/10%FBS solution. Samples were slowly triturated 30-100X with fire-polished Pasteur pipettes of decreasing bore size until fully suspended. Samples were then filtered, and flow sorted on a FACS ARIA-SORP sorter.

RNA sequencing

Total RNA was isolated from flow-sorted neurons using Trizol LS (Invitrogen) and the RNA Clean and Concentrator-5 kit (Zymo Research). RNA concentration and quality was determined using QuantiFluor RNA system (Promega) and Fragment analyzer (Advanced Analytics). Samples were converted to cDNA, depleted of rRNA transcripts, and amplified using the TRIO RNA-seq kit for mouse (Nugen Inc). Single-end sequencing was performed on a Nextseq 550 (Illumina) for 76 cycles. Read quality was assessed using FASTQC (<https://www.bioinformatics.babraham.ac.uk/projects/fastqc/>) and adapters were trimmed using Trimmomatic (Bolger et al., 2014). Filtered and trimmed reads were aligned to the mouse genome (mm10, UCSC) using Tophat2 (v2.1.1) (Kim et al., 2013).

RNA sequencing analysis

Gene expression quantification and differential expression were analyzed using Cufflinks v2.2.2 (Trapnell *et al.*, 2010). In all differential expression comparisons, a gene was called differentially expressed if fold-change was ≥ 1.5 and false discovery rate (FDR) was $\leq 5\%$. Hierarchical clustering of differentially expressed genes in rostral *Lmx1bcKO* and caudal *Lmx1bcKO* samples was performed in R (v. 3.5) using row-scaled values with Euclidean distance and complete linkage. The heatmap was plotted with the gplots library. Gene Ontology analysis was performed using Webgestalt (<http://www.webgestalt.org>), requiring five genes per category and FDR $\leq 5\%$. Venn diagrams were generated using BioVenn (<http://www.biovenn.nl>) (Hulsen *et al.*, 2008; Wang *et al.*, 2017). Differential exon expression analysis was performed to test for differences of the unique *Pcdhac2* first exon with DEXSeq (Anders *et al.*, 2012). RNA-seq reads were mapped to the *Mus musculus* genome (Ensembl, v. 96) and reads falling within annotated exons were counted using featureCounts (Rsubread). DEXSeq default settings were used and significant exon usage differences were determined at FDR $\leq 5\%$.

qPCR

RNA was isolated from YFP+ flow sorted cells in Trizol LS (Invitrogen) using chloroform extraction followed by the RNA Clean and Concentrator-5 kit (Zymo Research). cDNA was then synthesized using equal input RNA with the Transcriptor First Strand cDNA Synthesis Kit (Roche). cDNA was then amplified (8 PCR cycles) using PerfeCTa PreAmp SuperMix (QuantoBio) followed by Exol digest to remove excess primers. RT-qPCR was performed using PerfeCTa FastMix II ROX mastermix (QuantaBio) with TaqMan probes (ThermoFisher Scientific).

Chromatin immunoprecipitation analysis

ChIP-seq data for mycPet1 was obtained from Wyler *et al.* (2016). The data was re-analyzed using the ENCODE Transcription Factor ChIP-seq analysis pipeline (<https://github.com/ENCODE-DCC/chip-seq-pipeline>). Reads were mapped to the *Mus musculus* genome (UCSC mm10) using the Burroughs-Wheeler aligner (BWA) and peaks were called with MACS2 with FDR $\leq 1\%$ (Zhang *et al.*, 2008).

Axon quantification

Spinal cord: Coronal sections of spinal cords were taken at 25 μm . Two sections were taken blindly from each cervical and lumbar spinal segment from each genotype ($n = 3$, control; $n = 3$, *Lmx1bcKO* mice) and ($n = 3$, control; $n = 3$, *Pet1cKO*). Whole gray area or whole white matter area was selected independently, and pixels were quantified using Zeiss 2.3 Image Analysis module. Pixel values were normalized to selected area (μm^2) for each section. Two-way ANOVA with Welch's correction analysis was performed. p values for each comparison are detailed in Fig. Legends.

Forebrain: Coronal sections of hippocampus, cortex, and axon tracts (SCS and cingulum) were taken and TdTomato⁺ pixels were quantified using Zeiss 2.3 Image Analysis module in P3 targeted iControls ($n = 3$ non-littermate mice) and P3 *Lmx1bcKO* mice ($n = 3$ non-littermate mice). Pixel values were normalized to selected area (μm^2). Unpaired t-test with Welch's correction statistical analysis was performed. p values for each comparison are detailed in Fig. Legends.

Cell volume analysis

Thick tissue sections were sliced at 150 μm and cleared using CUBIC clearing technique to increase the optical transparency of sections (Susaki *et al.*, 2015). CUBIC reagent was prepared using urea (25 wt% final concentration), Quadrol (25 wt% final concentration), Triton X-100 (15 wt% final concentration) and dH₂O. Tissue sections were incubated in CUBIC reagent at 4°C overnight. To avoid the distortion of tissue by compression of the glass cover slip, Blu-Tack reusable adhesive was used to create a reservoir with a 0.3–0.5 mm depth. The transferred tissue sections were then sealed in CUBIC reagent using a glass cover slip for z-stack confocal imaging of the endogenous TdTomato fluorescence of cell bodies. The 3D neuron images were reconstructed and measured using the Surfaces or Filament Tracer tool in Imaris 7.4.2 (Bitplane, Zurich, Switzerland). Unpaired t-test with Welch's correction statistical analysis was performed. Sample size and p values for each comparison are detailed in Fig. Legends.

Image acquisition and processing

Immuno-stained slides were imaged on an LSM800 confocal microscope (Carl Zeiss). All embryonic forebrain images were captured using a BZ-X700 fluorescence microscope (Keyence) or Olympus Optical BX51 microscope. Global brightness and contrast were edited across whole images equally between genotypes. Whole sagittal sections (**Figure 1A,B**) were acquired using confocal 10X objective and both control and *Lmx1bcKO* sections were processed in ImageJ and subjected to equal background subtraction followed by Lookup Table-Fire to enhance visualization of TdTomato⁺ axon intensities in the forebrain. Axon tracing in **Figure 5D** and **Figure 9K** was performed using the *Filament Tracer* module in Imaris 7.4.2 (Bitplane, Zurich, Switzerland).

Accession codes

All data generated in this study are deposited in NCBI GEO under accession code GSE130514.

Acknowledgements

We thank Lynn Landmesser for key insights and suggestions throughout the course of this study. We thank Polyxeni Philippidou for her many helpful comments on the manuscript. We thank Wen-Cheng Xiong for the use of the BZ-X700 fluorescence microscope. We thank Randy Johnson for *Lmx1b* floxed mice. We thank Ralph Witzgall for the *Lmx1b* antibody. We thank Steven Wyler for the pup picture. This research was supported by the Genomics Core Facility and the Flow cytometry core at the CWRU School of Medicine. This research was supported by NIH grants P50 MH096972 and RO1 MH062723 to ESD.

Additional information

Funding

Funder	Grant reference number	Author
National Institute of Mental Health	P50 MH096972	Evan S Deneris
National Institute of Mental Health	RO1 MH062723	Evan S Deneris

The funders had no role in study design, data collection and interpretation, or the decision to submit the work for publication.

Author contributions

Lauren J Donovan, Conceptualization, Validation, Investigation, Interpretation of data; William C Spencer, Conceptualization, Data curation, Formal analysis, Validation, Investigation, Writing—original draft, Writing—review and editing, Interpretation of data; Meagan M Kitt, Investigation, Performed stereotaxic injection of rAAV2/Ef1a-DIO-hchr2-EYFP and in situ hybridization; Brent A Eastman, Investigation, Performed histochemical analysis and imaging of DKO mice; Katherine J Lobur, Investigation, Methodology; Kexin Jiao, Investigation, Methodology, Performed cell body morphological analyses and measurements, Performed Imaris tracing and imaging; Jerry Silver, Writing—review and editing, Interpretation of data; Evan S Deneris, Conceptualization, Supervision, Funding acquisition, Writing—original draft, Writing—review and editing, Interpretation of data

Author ORCIDs

Lauren J Donovan  <https://orcid.org/0000-0002-5622-7402>

William C Spencer  <https://orcid.org/0000-0002-9700-8011>

Evan S Deneris  <https://orcid.org/0000-0003-4211-9934>

Ethics

Animal experimentation: All animal procedures used in this study were in strict accordance with the Guide for the Care and Use of Laboratory Animals of the National Institutes of Health. The protocol

was approved by the Case Western Reserve University School of Medicine Institutional Animal Care and Use Committee (Animal Welfare Assurance Number A3145-01, protocol #: 2014-0044).

Decision letter and Author response

Decision letter <https://doi.org/10.7554/eLife.48788.027>

Author response <https://doi.org/10.7554/eLife.48788.028>

Additional files

Supplementary files

- Supplementary file 1. Legend Lmx1b-regulated axon-related genes in rostral and caudal 5-HT neurons at E17.5. Axon genes that are also regulated by Pet1 in rostral 5-HT neurons at E17.5 are in bold.

DOI: <https://doi.org/10.7554/eLife.48788.020>

- Transparent reporting form

DOI: <https://doi.org/10.7554/eLife.48788.021>

Data availability

Raw ChIP-seq data GEO accession: GSE74315. RNA-seq data generated in this study and ChIP-seq analysis are deposited in NCBI GEO under accession code GSE130514.

The following dataset was generated:

Author(s)	Year	Dataset title	Dataset URL	Database and Identifier
Donovan LJ, Spencer WC, Kitt MM, Eastman BA, Lobur KJ, Jiao K, Silver J, Deneris ES	2019	Lmx1b is required at multiple stages to build expansive serotonergic axon architectures	http://www.ncbi.nlm.nih.gov/geo/query/acc.cgi?acc=GSE130514	NCBI Gene Expression Omnibus, GSE130514

The following previously published dataset was used:

Author(s)	Year	Dataset title	Dataset URL	Database and Identifier
Wyler SC, Spencer WC, Green NH, Rood BD, Crawford L, Craige C, Gresch P, McMahon DG, Beck SG, Deneris ES	2016	Pet-1 Switches Transcriptional Targets Postnatally to Regulate Maturation of Serotonin Neuron Excitability.	http://www.ncbi.nlm.nih.gov/geo/query/acc.cgi?acc=GSE74315	NCBI Gene Expression Omnibus, GSE74315

References

- Anders S, Reyes A, Huber W. 2012. Detecting differential usage of exons from RNA-seq data. *Genome Research* **22**:2008–2017. DOI: <https://doi.org/10.1101/gr.133744.111>, PMID: 22722343
- Arlotta P, Molyneaux BJ, Chen J, Inoue J, Kominami R, Macklis JD. 2005. Neuronal subtype-specific genes that control corticospinal motor neuron development in vivo. *Neuron* **45**:207–221. DOI: <https://doi.org/10.1016/j.neuron.2004.12.036>, PMID: 15664173
- Azevedo FA, Carvalho LR, Grinberg LT, Farfel JM, Ferretti RE, Leite RE, Jacob Filho W, Lent R, Herculano-Houzel S. 2009. Equal numbers of neuronal and nonneuronal cells make the human brain an isometrically scaled-up primate brain. *The Journal of Comparative Neurology* **513**:532–541. DOI: <https://doi.org/10.1002/cne.21974>, PMID: 19226510
- Baker KG, Halliday GM, Halasz P, Hornung JP, Geffen LB, Cotton RG, Törk I. 1991. Cytoarchitecture of serotonin-synthesizing neurons in the pontine tegmentum of the human brain. *Synapse* **7**:301–320. DOI: <https://doi.org/10.1002/syn.890070407>, PMID: 2042112
- Ballion B, Branchereau P, Chapron J, Viala D. 2002. Ontogeny of descending serotonergic innervation and evidence for intraspinal 5-HT neurons in the mouse spinal cord. *Developmental Brain Research* **137**:81–88. DOI: [https://doi.org/10.1016/S0165-3806\(02\)00414-5](https://doi.org/10.1016/S0165-3806(02)00414-5), PMID: 12128257

- Bang SJ**, Jensen P, Dymecki SM, Commons KG. 2012. Projections and interconnections of genetically defined serotonin neurons in mice. *European Journal of Neuroscience* **35**:85–96. DOI: <https://doi.org/10.1111/j.1460-9568.2011.07936.x>, PMID: 22151329
- Bendotti C**, Servadio A, Samanin R. 1991. Distribution of GAP-43 mRNA in the brain stem of adult rats as evidenced by in situ hybridization: localization within monoaminergic neurons. *The Journal of Neuroscience* **11**: 600–607. DOI: <https://doi.org/10.1523/JNEUROSCI.11-03-00600.1991>, PMID: 1672151
- Björklund A**, Dunnett SB. 2007. Dopamine neuron systems in the brain: an update. *Trends in Neurosciences* **30**: 194–202. DOI: <https://doi.org/10.1016/j.tins.2007.03.006>, PMID: 17408759
- Bolger AM**, Lohse M, Usadel B. 2014. Trimmomatic: a flexible trimmer for illumina sequence data. *Bioinformatics* **30**:2114–2120. DOI: <https://doi.org/10.1093/bioinformatics/btu170>, PMID: 24695404
- Briscoe J**, Sussel L, Serup P, Hartigan-O'Connor D, Jessell TM, Rubenstein JL, Ericson J. 1999. Homeobox gene Nkx2.2 and specification of neuronal identity by graded Sonic hedgehog signalling. *Nature* **398**:622–627. DOI: <https://doi.org/10.1038/19315>, PMID: 10217145
- Chabrat A**, Brisson G, Doucet-Beaupré H, Salesse C, Schaan Profes M, Dovonou A, Akitegetse C, Charest J, Lemstra S, Côté D, Pasterkamp RJ, Abrudan MI, Metzakopian E, Ang SL, Lévesque M. 2017. Transcriptional repression of Plxn1 by Lmx1a and Lmx1b directs topographic dopaminergic circuit formation. *Nature Communications* **8**:933. DOI: <https://doi.org/10.1038/s41467-017-01042-0>, PMID: 29038581
- Chen B**, Schaevitz LR, McConnell SK. 2005. Fezl regulates the differentiation and axon targeting of layer 5 subcortical projection neurons in cerebral cortex. *PNAS* **102**:17184–17189. DOI: <https://doi.org/10.1073/pnas.0508732102>, PMID: 16284245
- Chen WV**, Nwakeze CL, Denny CA, O'Keeffe S, Rieger MA, Mountoufaris G, Kirner A, Dougherty JD, Hen R, Wu Q, Maniatis T. 2017. Pcdhcc2 is required for axonal tiling and assembly of serotonergic circuitries in mice. *Science* **356**:406–411. DOI: <https://doi.org/10.1126/science.aal3231>, PMID: 28450636
- Dai JX**, Han HL, Tian M, Cao J, Xiu JB, Song NN, Huang Y, Xu TL, Ding YQ, Xu L. 2008. Enhanced contextual fear memory in central serotonin-deficient mice. *PNAS* **105**:11981–11986. DOI: <https://doi.org/10.1073/pnas.0801329105>, PMID: 18695238
- Deneris E**, Gaspar P. 2018. Serotonin neuron development: shaping molecular and structural identities. *Wiley Interdisciplinary Reviews: Developmental Biology* **7**:e301. DOI: <https://doi.org/10.1002/wdev.301>, PMID: 29072810
- Deneris ES**, Hobert O. 2014. Maintenance of postmitotic neuronal cell identity. *Nature Neuroscience* **17**:899–907. DOI: <https://doi.org/10.1038/nn.3731>, PMID: 24929660
- Donovan SL**, Mamounas LA, Andrews AM, Blue ME, McCasland JS. 2002. GAP-43 is critical for normal development of the serotonergic innervation in forebrain. *The Journal of Neuroscience* **22**:3543–3552. DOI: <https://doi.org/10.1523/JNEUROSCI.22-09-03543.2002>, PMID: 11978831
- Fame RM**, MacDonald JL, Macklis JD. 2011. Development, specification, and diversity of callosal projection neurons. *Trends in Neurosciences* **34**:41–50. DOI: <https://doi.org/10.1016/j.tins.2010.10.002>, PMID: 21129791
- Fournet V**, Jany M, Fabre V, Chali F, Orsal D, Schweitzer A, Andrieux A, Messanvi F, Giros B, Hamon M, Lanfumey L, Deloulme JC, Martres MP. 2010. The deletion of the microtubule-associated STOP protein affects the serotonergic mouse brain network. *Journal of Neurochemistry* **115**:1579–1594. DOI: <https://doi.org/10.1111/j.1471-4159.2010.07064.x>, PMID: 20969568
- Fox SR**, Deneris ES. 2012. Engrailed is required in maturing serotonin neurons to regulate the cytoarchitecture and survival of the dorsal raphe nucleus. *Journal of Neuroscience* **32**:7832–7842. DOI: <https://doi.org/10.1523/JNEUROSCI.5829-11.2012>, PMID: 22674259
- Gagnon D**, Parent M. 2014. Distribution of VGLUT3 in highly collateralized axons from the rat dorsal raphe nucleus as revealed by single-neuron reconstructions. *PLOS ONE* **9**:e87709. DOI: <https://doi.org/10.1371/journal.pone.0087709>, PMID: 24504335
- Galazo MJ**, Emsley JG, Macklis JD. 2016. Corticothalamic projection neuron development beyond subtype specification: fog2 and intersectional controls regulate intraclass neuronal diversity. *Neuron* **91**:90–106. DOI: <https://doi.org/10.1016/j.neuron.2016.05.024>, PMID: 27321927
- Guillemot F**. 2007. Spatial and temporal specification of neural fates by transcription factor codes. *Development* **134**:3771–3780. DOI: <https://doi.org/10.1242/dev.006379>, PMID: 17898002
- Guo Y**, Monahan K, Wu H, Gertz J, Varley KE, Li W, Myers RM, Maniatis T, Wu Q. 2012. CTCF/cohesin-mediated DNA looping is required for protocadherin α promoter choice. *PNAS* **109**:21081–21086. DOI: <https://doi.org/10.1073/pnas.1219280110>, PMID: 23204437
- Haas HL**, Sergeeva OA, Selbach O. 2008. Histamine in the nervous system. *Physiological Reviews* **88**:1183–1241. DOI: <https://doi.org/10.1152/physrev.00043.2007>, PMID: 18626069
- Hannon J**, Hoyer D. 2008. Molecular biology of 5-HT receptors. *Behavioural Brain Research* **195**:198–213. DOI: <https://doi.org/10.1016/j.bbr.2008.03.020>, PMID: 18571247
- Hawthorne AL**, Wylie CJ, Landmesser LT, Deneris ES, Silver J. 2010. Serotonergic neurons migrate radially through the neuroepithelium by dynamin-mediated somal translocation. *Journal of Neuroscience* **30**:420–430. DOI: <https://doi.org/10.1523/JNEUROSCI.2333-09.2010>, PMID: 20071506
- Hawthorne AL**, Hu H, Kundu B, Steinmetz MP, Wylie CJ, Deneris ES, Silver J. 2011. The unusual response of serotonergic neurons after CNS injury: lack of axonal dieback and enhanced sprouting within the inhibitory environment of the glial scar. *Journal of Neuroscience* **31**:5605–5616. DOI: <https://doi.org/10.1523/JNEUROSCI.6663-10.2011>, PMID: 21490201
- Hendricks TJ**, Fyodorov DV, Wegman LJ, Lelutiu NB, Pehek EA, Yamamoto B, Silver J, Weeber EJ, Sweatt JD, Deneris ES. 2003. Pet-1 ETS gene plays a critical role in 5-HT neuron development and is required for normal

- anxiety-like and aggressive behavior. *Neuron* **37**:233–247. DOI: [https://doi.org/10.1016/S0896-6273\(02\)01167-4](https://doi.org/10.1016/S0896-6273(02)01167-4), PMID: 12546819
- Hobert O.** 2008. Regulatory logic of neuronal diversity: terminal selector genes and selector motifs. *PNAS* **105**: 20067–20071. DOI: <https://doi.org/10.1073/pnas.0806070105>, PMID: 19104055
- Hobert O.** 2016. Terminal selectors of neuronal identity. *Current Topics in Developmental Biology* **116**:455–475. DOI: <https://doi.org/10.1016/bs.ctdb.2015.12.007>, PMID: 26970634
- Hodges MR**, Wehner M, Aungst J, Smith JC, Richerson GB. 2009. Transgenic mice lacking serotonin neurons have severe apnea and high mortality during development. *Journal of Neuroscience* **29**:10341–10349. DOI: <https://doi.org/10.1523/JNEUROSCI.1963-09.2009>, PMID: 19692608
- Hornung JP.** 2003. The human raphe nuclei and the serotonergic system. *Journal of Chemical Neuroanatomy* **26**: 331–343. DOI: <https://doi.org/10.1016/j.jchemneu.2003.10.002>, PMID: 14729135
- Hulsen T**, de Vlieg J, Alkema W. 2008. BioVenn - a web application for the comparison and visualization of biological lists using area-proportional venn diagrams. *BMC Genomics* **9**:488. DOI: <https://doi.org/10.1186/1471-2164-9-488>, PMID: 18925949
- Jacob J**, Ferri AL, Milton C, Prin F, Pla P, Lin W, Gavalas A, Ang SL, Briscoe J. 2007. Transcriptional repression coordinates the temporal switch from motor to serotonergic neurogenesis. *Nature Neuroscience* **10**:1433–1439. DOI: <https://doi.org/10.1038/nn1985>, PMID: 17922007
- Jin Y**, Dougherty SE, Wood K, Sun L, Cudmore RH, Abdalla A, Kannan G, Pletnikov M, Hashemi P, Linden DJ. 2016. Regrowth of serotonin axons in the adult mouse brain following injury. *Neuron* **91**:748–762. DOI: <https://doi.org/10.1016/j.neuron.2016.07.024>, PMID: 27499084
- Katori S**, Hamada S, Noguchi Y, Fukuda E, Yamamoto T, Yamamoto H, Hasegawa S, Yagi T. 2009. Protocadherin-alpha family is required for serotonergic projections to appropriately innervate target brain Areas. *Journal of Neuroscience* **29**:9137–9147. DOI: <https://doi.org/10.1523/JNEUROSCI.5478-08.2009>, PMID: 19625505
- Katori S**, Noguchi-Katori Y, Okayama A, Kawamura Y, Luo W, Sakimura K, Hirabayashi T, Iwasato T, Yagi T. 2017. Protocadherin- α 2 is required for diffuse projections of serotonergic axons. *Scientific Reports* **7**:15908. DOI: <https://doi.org/10.1038/s41598-017-16120-y>, PMID: 29162883
- Kehayova P**, Monahan K, Chen W, Maniatis T. 2011. Regulatory elements required for the activation and repression of the protocadherin-alpha gene cluster. *PNAS* **108**:17195–17200. DOI: <https://doi.org/10.1073/pnas.1114357108>, PMID: 21949399
- Kim D**, Pertea G, Trapnell C, Pimentel H, Kelley R, Salzberg SL. 2013. TopHat2: accurate alignment of transcriptomes in the presence of insertions, deletions and gene fusions. *Genome Biology* **14**:R36. DOI: <https://doi.org/10.1186/gb-2013-14-4-r36>, PMID: 23618408
- Kim JY**, Kim A, Zhao ZQ, Liu XY, Chen ZF. 2014. Postnatal maintenance of the 5-Ht1a-Pet1 autoregulatory loop by serotonin in the raphe nuclei of the brainstem. *Molecular Brain* **7**:48. DOI: <https://doi.org/10.1186/1756-6606-7-48>, PMID: 24972638
- Kiyasova V**, Fernandez SP, Laine J, Stankovski L, Muzerelle A, Doly S, Gaspar P. 2011. A genetically defined morphologically and functionally unique subset of 5-HT neurons in the mouse raphe nuclei. *Journal of Neuroscience* **31**:2756–2768. DOI: <https://doi.org/10.1523/JNEUROSCI.4080-10.2011>, PMID: 21414898
- Laguna A**, Schintu N, Nobre A, Alvarsson A, Volakakis N, Jacobsen JK, Gómez-Galán M, Sopova E, Joodmardi E, Yoshitake T, Deng Q, Kehr J, Ericson J, Svenningsson P, Shupliakov O, Perlmann T. 2015. Dopaminergic control of autophagic-lysosomal function implicates Lmx1b in Parkinson's disease. *Nature Neuroscience* **18**:826–835. DOI: <https://doi.org/10.1038/nn.4004>
- Lee S**, Walker CL, Karten B, Kuny SL, Tennese AA, O'Neill MA, Wevrick R. 2005. Essential role for the Prader-Willi syndrome protein neclin in axonal outgrowth. *Human Molecular Genetics* **14**:627–637. DOI: <https://doi.org/10.1093/hmg/ddi059>, PMID: 15649943
- Lidov HG**, Molliver ME. 1982. An immunohistochemical study of serotonin neuron development in the rat: ascending pathways and terminal fields. *Brain Research Bulletin* **8**:389–430. DOI: [https://doi.org/10.1016/0361-9230\(82\)90077-6](https://doi.org/10.1016/0361-9230(82)90077-6), PMID: 6178481
- Liu C**, Maejima T, Wyler SC, Casadesus G, Herlitze S, Deneris ES. 2010. Pet-1 is required across different stages of life to regulate serotonergic function. *Nature Neuroscience* **13**:1190–1198. DOI: <https://doi.org/10.1038/nn.2623>, PMID: 20818386
- Livet J**, Sigrist M, Stroebel S, De Paola, Price SR, Henderson CE, Jessell TM, Arber S. 2002. ETS gene Pea3 controls the central position and terminal arborization of specific motor neuron pools. *Neuron* **35**:877–892. DOI: [https://doi.org/10.1016/S0896-6273\(02\)00863-2](https://doi.org/10.1016/S0896-6273(02)00863-2), PMID: 12372283
- Maddaloni G**, Bertero A, Pratelli M, Barsotti N, Boonstra A, Giorgi A, Migliarini S, Pasqualetti M. 2017. Development of serotonergic fibers in the Post-Natal mouse brain. *Frontiers in Cellular Neuroscience* **11**. DOI: <https://doi.org/10.3389/fncel.2017.00202>, PMID: 28769763
- Migliarini S**, Pacini G, Pelosi B, Lunardi G, Pasqualetti M. 2013. Lack of brain serotonin affects postnatal development and serotonergic neuronal circuitry formation. *Molecular Psychiatry* **18**:1106–1118. DOI: <https://doi.org/10.1038/mp.2012.128>, PMID: 23007167
- Moore RY**, Bloom FE. 1979. Central catecholamine neuron systems: anatomy and physiology of the norepinephrine and epinephrine systems. *Annual Review of Neuroscience* **2**:113–168. DOI: <https://doi.org/10.1146/annurev.ne.02.030179.000553>, PMID: 231924
- Muzerelle A**, Scotto-Lomassese S, Bernard JF, Soiza-Reilly M, Gaspar P. 2016. Conditional anterograde tracing reveals distinct targeting of individual serotonin cell groups (B5-B9) to the forebrain and brainstem. *Brain Structure and Function* **221**:535–561. DOI: <https://doi.org/10.1007/s00429-014-0924-4>, PMID: 25403254

- Okaty BW**, Freret ME, Rood BD, Brust RD, Hennessy ML, deBairos D, Kim JC, Cook MN, Dymecki SM. 2015. Multi-Scale molecular deconstruction of the serotonin neuron system. *Neuron* **88**:774–791. DOI: <https://doi.org/10.1016/j.neuron.2015.10.007>, PMID: 26549332
- Paolino A**, Fenlon LR, Suárez R, Richards LJ. 2018. Transcriptional control of long-range cortical projections. *Current Opinion in Neurobiology* **53**:57–65. DOI: <https://doi.org/10.1016/j.conb.2018.05.005>, PMID: 29894898
- Pattyn A**, Simplicio N, van Doorninck JH, Goridis C, Guillemot F, Brunet JF. 2004. Ascl1/Mash1 is required for the development of central serotonergic neurons. *Nature Neuroscience* **7**:589–595. DOI: <https://doi.org/10.1038/nn1247>, PMID: 15133515
- Rajaofetra N**, Sandillon F, Geffard M, Privat A. 1989. Pre- and post-natal ontogeny of serotonergic projections to the rat spinal cord. *Journal of Neuroscience Research* **22**:305–321. DOI: <https://doi.org/10.1002/jnr.490220311>, PMID: 2709447
- Ren J**, Friedmann D, Xiong J, Liu CD, Ferguson BR, Weerakkody T, DeLoach KE, Ran C, Pun A, Sun Y, Weissbourd B, Neve RL, Huguenard J, Horowitz MA, Luo L. 2018. Anatomically defined and functionally distinct dorsal raphe serotonin Sub-systems. *Cell* **175**:472–487. DOI: <https://doi.org/10.1016/j.cell.2018.07.043>
- Ribich S**, Tasic B, Maniatis T. 2006. Identification of long-range regulatory elements in the protocadherin-alpha gene cluster. *PNAS* **103**:19719–19724. DOI: <https://doi.org/10.1073/pnas.0609445104>, PMID: 17172445
- Santiago C**, Bashaw GJ. 2014. Transcription factors and effectors that regulate neuronal morphology. *Development* **141**:4667–4680. DOI: <https://doi.org/10.1242/dev.110817>, PMID: 25468936
- Scott MM**, Wylie CJ, Lerch JK, Murphy R, Lobur K, Herlitze S, Jiang W, Conlon RA, Strowbridge BW, Deneris ES. 2005. A genetic approach to access serotonin neurons for in vivo and in vitro studies. *PNAS* **102**:16472–16477. DOI: <https://doi.org/10.1073/pnas.0504510102>, PMID: 16251278
- Shen Y**, Mani S, Donovan SL, Schwob JE, Meiri KF. 2002. Growth-associated protein-43 is required for commissural axon guidance in the developing vertebrate nervous system. *The Journal of Neuroscience* **22**:239–247. DOI: <https://doi.org/10.1523/JNEUROSCI.22-01-00239.2002>, PMID: 11756507
- Shirasaki R**, Pfaff SL. 2002. Transcriptional codes and the control of neuronal identity. *Annual Review of Neuroscience* **25**:251–281. DOI: <https://doi.org/10.1146/annurev.neuro.25.112701.142916>, PMID: 12052910
- Srivatsa S**, Parthasarathy S, Molnár Z, Tarabykin V. 2015. Sip1 downstream effector ninein controls neocortical axonal growth, ipsilateral branching, and microtubule growth and stability. *Neuron* **85**:998–1012. DOI: <https://doi.org/10.1016/j.neuron.2015.01.018>, PMID: 25741725
- Steinbusch HW**. 1981. Distribution of serotonin-immunoreactivity in the central nervous system of the rat-cell bodies and terminals. *Neuroscience* **6**:557–618. DOI: [https://doi.org/10.1016/0306-4522\(81\)90146-9](https://doi.org/10.1016/0306-4522(81)90146-9), PMID: 7017455
- Suleiman H**, Heudobler D, Raschta AS, Zhao Y, Zhao Q, Hertting I, Vitzthum H, Moeller MJ, Holzman LB, Rachel R, Johnson R, Westphal H, Raschle A, Witzgall R. 2007. The podocyte-specific inactivation of Lmx1b, Ldb1 and E2a yields new insight into a transcriptional network in podocytes. *Developmental Biology* **304**:701–712. DOI: <https://doi.org/10.1016/j.ydbio.2007.01.020>, PMID: 17316599
- Susaki EA**, Tainaka K, Perrin D, Yukinaga H, Kuno A, Ueda HR. 2015. Advanced CUBIC protocols for whole-brain and whole-body clearing and imaging. *Nature Protocols* **10**:1709–1727. DOI: <https://doi.org/10.1038/nprot.2015.085>, PMID: 26448360
- Trapnell C**, Williams BA, Pertea G, Mortazavi A, Kwan G, van Baren MJ, Salzberg SL, Wold BJ, Pachter L. 2010. Transcript assembly and quantification by RNA-Seq reveals unannotated transcripts and isoform switching during cell differentiation. *Nature Biotechnology* **28**:511–515. DOI: <https://doi.org/10.1038/nbt.1621>, PMID: 20436464
- van Doorninck JH**, van Der Wees J, Karis A, Goedknegt E, Engel JD, Coesmans M, Rutteman M, Grosveld F, De Zeeuw CI. 1999. GATA-3 is involved in the development of serotonergic neurons in the caudal raphe nuclei. *The Journal of Neuroscience* **19**:RC12. DOI: <https://doi.org/10.1523/JNEUROSCI.19-12-j0002.1999>, PMID: 10366650
- Wang J**, Vasaikar S, Shi Z, Greer M, Zhang B. 2017. WebGestalt 2017: a more comprehensive, powerful, flexible and interactive gene set enrichment analysis toolkit. *Nucleic Acids Research* **45**:W130–W137. DOI: <https://doi.org/10.1093/nar/gkx356>, PMID: 28472511
- Wei GH**, Badis G, Berger MF, Kivioja T, Palin K, Enge M, Bonke M, Jolma A, Varjosalo M, Gehrke AR, Yan J, Talukder S, Turunen M, Taipale M, Stunnenberg HG, Ukkonen E, Hughes TR, Bulky ML, Taipale J. 2010. Genome-wide analysis of ETS-family DNA-binding in vitro and in vivo. *The EMBO Journal* **29**:2147–2160. DOI: <https://doi.org/10.1038/emboj.2010.106>, PMID: 20517297
- Wyler SC**, Spencer WC, Green NH, Rood BD, Crawford L, Craige C, Gresch P, McMahon DG, Beck SG, Deneris E. 2016. Pet-1 switches transcriptional targets postnatally to regulate maturation of serotonin neuron excitability. *The Journal of Neuroscience* **36**:1758–1774. DOI: <https://doi.org/10.1523/JNEUROSCI.3798-15.2016>, PMID: 26843655
- Yan CH**, Levesque M, Claxton S, Johnson RL, Ang SL. 2011. Lmx1a and Lmx1b function cooperatively to regulate proliferation, specification, and differentiation of midbrain dopaminergic progenitors. *Journal of Neuroscience* **31**:12413–12425. DOI: <https://doi.org/10.1523/JNEUROSCI.1077-11.2011>, PMID: 21880902
- Zhang Y**, Liu T, Meyer CA, Eeckhoutte J, Johnson DS, Bernstein BE, Nusbaum C, Myers RM, Brown M, Li W, Liu XS. 2008. Model-based analysis of ChIP-Seq (MACS). *Genome Biology* **9**:R137. DOI: <https://doi.org/10.1186/gb-2008-9-9-r137>, PMID: 18798982
- Zhang X**, Yan H, Luo Y, Huang Z, Rao Y. 2018. Thermoregulation-Independent regulation of sleep by serotonin revealed in mice defective in serotonin synthesis. *Molecular Pharmacology* **93**:657–664. DOI: <https://doi.org/10.1124/mol.117.111229>, PMID: 29632139

- Zhao ZQ**, Scott M, Chiechio S, Wang JS, Renner KJ, Gereau RW, Johnson RL, Deneris ES, Chen ZF. 2006. Lmx1b is required for maintenance of central serotonergic neurons and mice lacking central serotonergic system exhibit normal locomotor activity. *Journal of Neuroscience* **26**:12781–12788. DOI: <https://doi.org/10.1523/JNEUROSCI.4143-06.2006>, PMID: 17151281
- Zhao ZQ**, Chiechio S, Sun YG, Zhang KH, Zhao CS, Scott M, Johnson RL, Deneris ES, Renner KJ, Gereau RW, Chen ZF. 2007a. Mice lacking central serotonergic neurons show enhanced inflammatory pain and an impaired analgesic response to antidepressant drugs. *Journal of Neuroscience* **27**:6045–6053. DOI: <https://doi.org/10.1523/JNEUROSCI.1623-07.2007>, PMID: 17537976
- Zhao ZQ**, Gao YJ, Sun YG, Zhao CS, Gereau RW, Chen ZF. 2007b. Central serotonergic neurons are differentially required for opioid analgesia but not for morphine tolerance or morphine reward. *PNAS* **104**:14519–14524. DOI: <https://doi.org/10.1073/pnas.0705740104>, PMID: 17724336